

Curriculum-Guided Antifragile Reinforcement Learning for Secure UAV Deconfliction under Observation-Space Attacks

Deepak Kumar Panda, Adolfo Perrusquía and Weisi Guo

Abstract—Reinforcement learning (RL) policies deployed in safety-critical systems, such as unmanned aerial vehicle (UAV) navigation in dynamic airspace, are vulnerable to out-of-distribution (OOD) adversarial attacks in the observation space. These attacks induce distributional shifts that significantly degrade value estimation, leading to unsafe or suboptimal decision-making rendering the existing policy fragile. To address this vulnerability, we propose an antifragile RL framework designed to adapt against curriculum of incremental adversarial perturbations. The framework introduces a simulated attacker which incrementally increases the strength of observation-space perturbations which enables the RL agent to adapt and generalize across a wider range of OOD observations and anticipate previously unseen attacks. We begin with a theoretical characterization of fragility, formally defining catastrophic forgetting as a monotonic divergence in value function distributions with increasing perturbation strength. Building on this, we define antifragility as the boundedness of such value shifts and derive adaptation conditions under which forgetting is stabilized. Our method enforces these bounds through iterative expert-guided critic alignment using Wasserstein distance minimization across incrementally perturbed observations. We empirically evaluate the approach in a UAV deconfliction scenario involving dynamic 3D obstacles. Results show that the antifragile policy consistently outperforms standard and robust RL baselines when subjected to both projected gradient descent (PGD) and GPS spoofing attacks, achieving up to 15% higher cumulative reward and over 30% fewer conflict events. These findings demonstrate the practical and theoretical viability of antifragile reinforcement learning for secure and resilient decision-making in environments with evolving threat scenarios.

Index Terms—Catastrophic forgetting, antifragility, unsupervised adaptation, adversarial, reinforcement learning

I. INTRODUCTION

Fragility, robustness, and antifragility represent a continuum of system responses to stress or external perturbations [1, 2]. Fragile systems degrade under stress, robust systems withstand disruption without structural change, and antifragile systems adaptively improve when exposed to uncertainty or adversity. In the context of autonomous systems like UAV navigation, these properties translate into how learning systems behave under known and unknown adversarial influence.

This work was supported by the Royal Academy of Engineering and the Office of the Chief Science Adviser for National Security under the UK Intelligence Community Postdoctoral Research Fellowship programme

¹D. Kumar Panda, A. Perrusquía and W. Guo are with the Faculty of Engineering and Applied Sciences, Cranfield University, MK43 0AL Cranfield, U.K. Deepak.Panda@cranfield.ac.uk, Adolfo.Perrusquia-Guzman@cranfield.ac.uk, weisi.guo@cranfield.ac.uk

Unmanned aerial vehicles (UAVs) are increasingly deployed across critical civilian domains such as logistics, surveillance, and disaster response [3]. These applications rely on autonomous path-planning algorithms that enable UAVs to navigate complex and dynamic environments. Path planning strategies typically fall into two categories: strategic and tactical [4, 5]. Strategic planning leverages global knowledge of the environment to generate optimized flight paths that prioritize path-length efficiency and obstacle avoidance. However, such approaches do not have the flexibility to adapt to real-time events, such as sudden weather changes, unexpected obstacles, or mission updates. In contrast, tactical or dynamic path planning relies on onboard sensors such as LiDAR, GPS, cameras, and radar [6, 7] to support reactive decision-making during flight. Within this paradigm, automatic dependent surveillance–broadcast (ADS-B)—a satellite-based GPS broadcasting protocol—is commonly adopted in unmanned traffic management (UTM) systems [8] due to its global coverage, low cost, energy efficiency, and real-time data transmission capabilities [9, 10]. However, ADS-B signals are unauthenticated and unencrypted, making them susceptible to spoofing [11, 12] and jamming attacks [13]. This raises concerns for UAVs that depend on ADS-B for safe in-flight navigation.

To address these vulnerabilities, RL has emerged as a model-free alternative for adaptive path planning in dynamic environments [14, 15]. RL policies can be deployed in the cloud or embedded into onboard firmware, but both implementation techniques introduce new attack vectors. These include cloud-side vulnerabilities [16], firmware tampering [17], and policy reconstruction via imitation learning techniques such as behavior cloning or generative adversarial imitation learning (GAIL) [18]. If adversaries reconstruct the policy or gain access to it and use it to spoof sensor inputs, they may disrupt UAV mission by inducing suboptimal decisions, unsafe paths, or excessive energy consumption [19, 20]. Despite the use of RL in adversarial environments, current methods lack theoretical guarantees under input-space attacks and fail to adapt under worsening perturbation, motivating the need for antifragile policy learning frameworks.

A. Related Works

1) *Antifragile Learning*: Robust RL has received significant attention as a means to enhance the resilience of agents against adversarial attacks and environmental uncertainty. Prior work

has explored various forms of robust training, including adversarial data augmentation, distributional robustness, and action-noise modeling, to improve safety in critical applications such as air mobility and autonomous navigation [12, 21–23]. However, these methods typically assume bounded perturbations or static adversaries and rely on fixed policy responses, thus limiting their adaptability to new or evolving threats. As a result, robust agents often generalize poorly when exposed to unmodeled or unseen adversarial scenarios. Advancing from robustness toward antifragility requires agents not only to resist disruptions, but to adapt and improve under adversarial attacks. The adaptation and improvement requires continual policy evolution that enables the agent to utilize the adversarial observations to improve its decision-making capabilities. Early efforts in this direction include antifragile control methods based on sliding-mode techniques [24] and RL under environmental disturbances [25]. Similarly, fragility and antifragility characteristics in deep neural networks have been investigated through synaptic filters to assess learning behavior under adversarial attacks [26]. However, existing computational frameworks for antifragility fail to integrate or preserve robustness formally.

As argued by [1] antifragility must build upon an underlying layer of robustness to ensure system adaptation does not compromise operational metrics. This is especially critical in domains such as UAV navigation in UTM, where system degradation can lead to severe operational consequences. Yet the antifragile learning methods proposed in [2, 24–26] largely treat robustness and antifragility in isolation, without providing guarantees for robust policy behavior under adversarial conditions. More recently, the concept of expanding robustness boundaries has been introduced through mechanisms such as safe exploration and adaptive policy refinement [27]. These approaches support antifragility by encouraging risk-aware adaptation while preserving essential operational constraints.

2) *Unsupervised Domain Adaptation*: In the context of adversarial learning for autonomous agents, unsupervised domain adaptation (UDA) offers a promising direction for transferring policies across perturbed observation distributions without requiring new labels, especially amongst domains with differing data distributions [28]. Key challenge in UDA is reducing distributional mismatch, often by learning domain-invariant representations or aligning latent features across domains [29]. Common approaches include adversarial generative alignment [30, 31], minimization of divergence-based metrics such as maximum mean discrepancy (MMD) or Wasserstein distance [32, 33], and shared latent embedding techniques for policy transfer in RL [34].

In the RL setting, domain adaptation becomes relevant for problems involving sim-to-real transfer or curriculum learning, where the environment undergoes gradual or structured changes [33, 35]. Various strategies have been proposed, including meta-learning [36], model regularization [37], and auxiliary loss functions to preserve performance on the source domain [38]. However, many of these approaches suffer from catastrophic forgetting, particularly when the target domain deviates significantly or involves adversarial perturbations. Forgetting arises from the instability of learned value functions

across evolving state-space distribution, and from overfitting to the new domain without preserving performance in the original one [39, 40]. Although forgetting has been mitigated through neuron restoration, pseudo-replay, or use of pre-trained encoders [38, 41], these methods are primarily designed for task-level continual learning and do not directly address adversarial distribution shifts that disrupt value estimation in RL. Adversarial transitions pose unique challenges: they often lead to systematic underestimation of value distributions and amplify policy drift, which can have catastrophic consequences in safety-critical systems like UAVs [42]. Recent works have explored expert-guided adaptation and experience replay using combined online and offline data to improve robustness in adversarial RL settings [43, 44]. However, these efforts do not explicitly leverage expert critic alignment for domain adaptation in adversarial observation spaces, nor do they provide theoretical guarantees on value stability during transfer.

Moreover, it is essential to distinguish catastrophic forgetting due to adversarial inputs from that in task-driven continual learning. In the adversarial case, the forgetting results from distributional shifts induced by attacks that distort observed states, rather than from sequential task changes. Moreover, existing UDA techniques are vulnerable to adversarial input perturbations, which violate key assumptions such as domain smoothness or label invariance—making them insufficient for secure policy transfer. This distinction motivates the need for novel antifragile RL frameworks to incorporate curriculum-based adaptation over adversarial perturbation levels. Unlike prior works that align latent features via adversarial loss or KL divergence, our method stabilizes value predictions directly via expert critic alignment. This enables adaptation across adversarial perturbation levels without overfitting to transient attack features.

B. Contributions and Outline

Despite recent progress in robust and adversarial RL, critical gaps remain in enabling autonomous agents to adapt securely under evolving observation-space attacks. Two key limitations are identified in the current state-of-the-art; 1) *Catastrophic forgetting in adversarial RL is underexplored*. While RL agents are known to degrade under adversarial observations, the underlying mechanisms of forgetting—particularly how value estimates diverge as perturbation strength increases—remain poorly understood. This limits the development of theoretically grounded defenses. 2) *Existing antifragile learning approaches lack robustness integration* violating the fragility–robustness–antifragility continuum proposed by Taleb [1]. In safety-critical domains like UAV navigation in UTM, antifragile adaptation must build on robust decision-making under sensor spoofing attacks. To address these gaps, we propose a novel antifragile RL framework that supports secure policy adaptation under adversarial observation-space attacks. The framework incorporates curriculum-guided unsupervised domain adaptation driven by expert critic alignment. Specifically, a policy trained using robust RL under nominal or low-intensity perturbations is reused as an expert to guide learning at progressively stronger attack levels. This adaptation

process is formalized through a bounded minimization of the distributional distance—measured via the Wasserstein-1 metric—between TD-error distributions across perturbation domains. To prevent overfitting and improve generalization, adversarial samples are introduced incrementally via a curriculum learning strategy [33], simulating a gradual attack escalation. This supports a value-aligned, policy-stable learning trajectory that avoids catastrophic forgetting while enabling antifragile adaptation. The methodology parallels the philosophy of learning from imperfect demonstrations [45, 46], and aligns with domain-informed defenses in adversarial ML [47]. The overall framework is depicted in Figure 1. In contrast to conventional robust learning, antifragile RL adapts to adversarial influence by leveraging it for value realignment. This property makes the proposed approach particularly suitable for deployment in security-sensitive domains such as UAV navigation in contested airspace, where sustained adversarial inputs—such as GPS spoofing or adversarial trajectory manipulation—may otherwise lead to policy degradation or mission failure. The main contributions of this work are summarized as follows.

- **A formal definition and analysis of catastrophic forgetting under adversarial perturbations:** We conceptualize forgetting in RL as a distributional divergence in temporal difference (TD) errors. Using the Wasserstein-1 distance, we provide a metric to quantify the degradation in learned value functions caused by observation-space attacks.
- **A theoretical framework for antifragile learning with bounded forgetting guarantees:** We prove that non-adaptive policies suffer from monotonically increasing forgetting as adversarial strength grows. To counter this, we introduce an antifragile policy framework that aligns its value function with expert critics trained under milder adversarial settings which formally bounds the TD-error shift between incremental attack stages, offering a quantifiable guarantee of value function stability.
- **Empirical validation in a 3D UAV deconfliction task under spoofing and PGD attacks:** We benchmark our method in a high-fidelity simulation of UAV conflict resolution with 3D obstacles under adversarial influence. Results demonstrate significant improvements in both safety (conflict-free navigation) and reward retention when compared to standard and robust RL baselines like adversarial meta, action robust RL and state-observation perturbation RL respectively.

The outline of the paper is as follows. Section II describes the UAV deconfliction agent in UTM proposed in this work. Section III introduces the RL action-robust action approach to obtain the expert critic for antifragile adaptation. In section IV the definition of fragility and antifragility is defined with respect to catastrophic forgetting and theoretical bounds are derived for antifragile learning. Section V reports on the simulation studies and the conclusions are presented in Section VI.

C. Notations and Preliminaries

Throughout this paper, \mathbb{R} , \mathbb{R}^n denote sets of natural numbers, real numbers, and real vectors of dimensions n —, respectively. In the standard DDPG algorithm, the policy network π_θ , parameterized by θ , and the critic network Q_ϕ , parameterized by ϕ , are used. The RL agent (RL) selects actions a' in the time t step using the policy π_θ , leading to a state transition to Φ^{t+1} and obtaining the reward r' . The goal of DDPG is to optimize the parameters $\{\phi, \theta\}$ of the critic and policy networks to maximize the episodic discounted return, defined as $R_{ep} = \sum_{t=1}^T \gamma^t r^t$, where $\gamma \in (0, 1)$ is the discount factor. In action robust DDPG (AR-DDPG), the framework, extends this set-up by introducing both the agent policy network $\pi_\theta^{\text{agent}}$ and an adversarial policy network π_θ^{adv} , which are trained using a shared critic Q_{AR} . The adverse states, Φ_{adv}^e , are generated with a perturbation magnitude $\varepsilon > 0$, calculated using the gradient of the actor loss function with respect to the input state $\Delta_{\Phi^t} \mathcal{L}_{\text{actor}}$. The model then incorporates adaptation using expert data through the critic Q_{exp} . For distributional adaptation, the 1-Wasserstein loss $\mathcal{W}_1(\cdot)$ is utilized to effectively align the state-action-value distribution. During antifragile adaptation, π_{ε_k} represents the policy under the adversarial attack of strength ε_k .

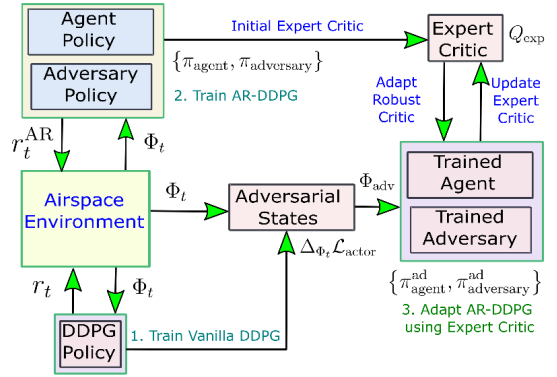


Fig. 1. The schematic for antifragile learning incorporating expert critic induced domain adaptation against adversarial states for action robust RL.

Fig. 1 describes the proposed framework which consists in the following four main steps,

- **Step 1: Training the DDPG policy** The policy network, π_θ , is trained using the DDPG algorithm to establish a baseline policy.
- **Step 2: Obtain action robust policies** Action-robust policies are derived by training multiple agent and adversarial policies, introducing perturbations in the overall action space. The optimal α is selected based on minimizing catastrophic forgetting in policies that result from adversarial attacks. Furthermore, expert data are extracted from the most robust policies that are vulnerable to adversarial attacks of lower intensity.
- **Step 3: Generating adversarial observations** Adversarial perturbations are generated using the actor policies π_θ from the DDPG. These perturbations are designed to exclude redundant states, thus mitigating policy overfitting and enhancing adversarial robustness.

- **Step 4: Action robust policy adaptation for an-tifragility** The critic component of the robust RL framework is adapted using iteratively updated expert data using a curriculum of adversarial states of increasing strength.

In order to develop the above scheme, first we consider the UAV deconfliction for UTM environment as explained in the next section.

II. UAV DECONFLICTION ENVIRONMENT

1) *Transition Model*: RL is used to plan point-to-point airspace navigation while avoiding predefined 3D obstacle trajectories. In this context, UAV navigation is influenced by the kinematics and geometry of 3D obstacles, which generate a repulsive force that disrupts the attractive flow field guiding the UAV toward its target. Effective navigation requires balancing these opposing forces to ensure successful mission completion. The attractive and repulsive fields have been formulated as per [48]. First, the attractive field between the UAV and its target destination point is determined. Let the UAV's position vector be $P = (x, y, z)$, and its corresponding velocity be denoted as $v(P)$. The velocity is computed as follows:

$$v(P) = - \left[\frac{C(x - x_d)}{d(P, P_g)}, \frac{C(y - y_d)}{d(P, P_g)}, \frac{C(z - z_d)}{d(P, P_g)} \right]^T. \quad (1)$$

Here, C represents a scaling constant, $P_g = (x_d, y_d, z_d)$ is the target position, and $d(P, P_g)$ denotes the Euclidean distance between the current position of the UAV and its target. Consider the velocity of an obstacle at the position of the UAV P , denoted by $v_{\text{obs}}(P)$. The resulting velocity of the UAV, influenced by the disturbance in the attractive flow field caused by the repulsive flow field of the obstacles expressed as

$$\bar{v}(P) = \bar{M}(\rho, \zeta, \varphi) [v(P) - v_{\text{obs}}(P)] + v_{\text{obs}}(P), \quad (2)$$

where, $\bar{M}(\rho, \zeta, \varphi)$ represents the modulation function that accounts for the interaction between the desired velocity of the UAV toward the target destination and the obstacle-induced velocity, using the parameters ρ , ζ and φ as detailed in [48] provided in Appendix A. σ controls the repulsive force from obstacles, ρ adjusts the attractive force toward the goal, and φ refers to the direction of the UAV. The UAV position update during the time interval ΔT , based on its velocity from (2) is given by:

$$P^{t+1} = P^t + \bar{v}(P^t) \Delta T. \quad (3)$$

The model in (3) acts as the UAV's transition model when an action (ρ, ζ, φ) is chosen from the RL policies, thus updating its position in the next time-step. The input states Φ based on which the control action is taken are explained in the next subsection.

2) *States*: The UAV, equipped with an RL agent for navigation, receives real-time information through ADS-B in the UTM environment [49] from other moving obstacles similar to a UAV with fixed trajectory required for tasks such as infrastructure inspection [50], road traffic monitoring, and surveillance [51]. The UAV obtains the position of the obstacle P_{obs}^t and the velocity v_{obs}^t at time t . The position of the UAV P^t

is assumed to be obtained from the built-in ADS-B sensor, via GPS location. The agent input state at the time t includes the UAV's relative position to both the target and nearby obstacles, which is formally represented as

$$\Phi^t = \{P_g - P^t, P_{\text{obs}}^t - P^t, v_{\text{obs}}^t\}. \quad (4)$$

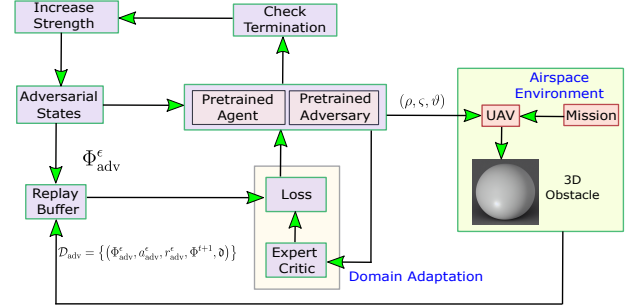


Fig. 2. The adaptation scheme for the action robust RL policies against incremental adversarial observations using expert data.

3) *Actions*: The actions of the UAV, as illustrated in Fig. 2, are represented by the vector $a_t = (\rho, \zeta, \vartheta)$, where:

- (ρ, ζ) determine the influence of the repulsive force of the obstacles and the attractive force toward the target, respectively, on UAV navigation.
- φ denotes the heading angle that the UAV must adjust to reach the designated destination.

4) *Reward*: The agent reward for a given state Φ_t upon selecting the action a_t is given by,

$$R^t(a^t | \Phi^t) = \lambda_1 \cdot R_1 + \lambda_2 \cdot R_2 + \lambda_3 \cdot R_3. \quad (5)$$

where, $\lambda_1, \lambda_2, \lambda_3 > 0$ are weighing factors. Each reward component R_1, R_2 , and R_3 is defined as follows

- **Penalty Reward (R_1)** that penalizes the agent if the transitioned position P^{t+1} falls within a certain radius of the dynamic obstacle, as represented by:

$$R_1 = \frac{\|P^{t+1} - P_{\text{obs}}\|}{R_{\text{obs}}}, \quad \text{if } \|P^{t+1} - P_{\text{obs}}\| \leq R_{\text{obs}}. \quad (6)$$

where, R_{obs} represents the radius around the obstacle.

- **Path Optimization Reward (R_2)** that incentivizes path optimization, while considering the proximity to the goal and the obstacles:

$$R_2 = \begin{cases} -\frac{\|P^{t+1} - P_g\|}{\|P_{\text{obs}} - P_g\|}, & \text{if } \|P^{t+1} - P_g\| > \varepsilon, \\ -\frac{\|P^{t+1} - P_g\|}{\|P_{\text{obs}} - P_g\|} + C_1, & \text{if } \|P^{t+1} - P_g\| \leq \varepsilon. \end{cases} \quad (7)$$

In (7), ε refers to the threshold margin for the reward R_2 .

- **Obstacle Threat Penalty (R_3)** imposing a penalty if the planned trajectory intersects a defined threat zone around an obstacle:

$$R_3 = \frac{\|P^{t+1} - P_{\text{obs}} - (R_{\text{obs}} + r)\|}{R_{\text{obs}}} - C_2, \quad (8)$$

if $R_{\text{obs}} < \|P^{t+1} - O_{\text{obs}}\| < R_{\text{obs}} + r$.

III. EXPERT CRITIC FORMULATION VIA ACTION ROBUST RL

As illustrated in Fig. 1, the initial robust RL is developed, compensating the fixed distributional shift in the observation with adversarial policies. It involves the concurrent design and training of the adversarial policy $\pi_{\omega}^{\text{adv}}$ and the agent policy $\pi_{\theta}^{\text{agent}}$ which are parameterized by $\{\omega, \theta\}$, respectively. Both policies share a common critic function, $Q_{\text{AR}}(\Phi^t, a^t)$ parameterized by ϕ . The adversarial policies, represented by $\pi_{\omega}^{\text{adv}}$, introduce perturbations to the action space, controlled by the parameter $\alpha \in [0, 1]$. When the action a_t is executed in the environment, the agent receives the reward r_t , as detailed in subsection II-4. This results in the agent state transitioning from Φ^t to Φ^{t+1} , as described in (3). The experience $e_t = (\Phi^t, a^t, r^t, \Phi^{t+1})$ is then stored in the replay buffer \mathcal{D} . A batch of experiences, $\mathcal{D}_{\text{batch}} = (e_1, \dots, e_N)$, is sampled to train the shared critic function $Q_{\text{AR}}(\Phi^t, a^t)$, which is used to update both the agent policy $\pi_{\theta}^{\text{agent}}$ and the adversarial policy $\pi_{\omega}^{\text{adv}}$. The agent and adversarial policies are trained while considering a two-player Markov game, as explained in the following subsection. The two-player Markov game formulation instead of MDP, helps in obtaining the action-robust policy under a bound state perturbation. A two-player zero-sum Markov game [52] is considered, where at each time step, both the agent and the adversary select an action concurrently. The reward at time t depends on the state Φ^t and the joint action a^t , which consists of the actions of both players and governs the transition dynamics. The game is modeled as a Markov decision process (MDP) $\mathcal{M}_2 = (\mathcal{S}, \mathcal{A}_{\text{agent}}, \mathcal{A}_{\text{adv}}, T_2, \gamma, R_2, P_0)$, where $\mathcal{A}_{\text{agent}}$ and \mathcal{A}_{adv} represent the continuous action space for the agent and adversary policies, respectively. T_2 represents the transition function, P_0 represents the transition probability function, while R_2 represents the reward function. The state transition function is given by $T_2 : \mathcal{S} \times \mathcal{A}_{\text{agent}} \times \mathcal{A}_{\text{adv}} \times \mathcal{S} \rightarrow \mathbb{R}$, and the reward function is defined by $R_2 : \mathcal{S} \times \mathcal{A}_{\text{agent}} \times \mathcal{A}_{\text{adv}} \rightarrow \mathbb{R}$. In this framework, the agent follows the policy $\pi_{\theta}^{\text{agent}} : \mathcal{S} \rightarrow \mathcal{A}_{\text{agent}}$ and the adversary follows the policy $\pi_{\omega}^{\text{adv}} : \mathcal{S} \rightarrow \mathcal{A}_{\text{adv}}$. At each time step, t , both players observe the state Φ^t , and their respective actions are given by $a_{\text{agent}}^t = \pi_{\theta}^{\text{agent}}(\Phi^t)$ and $a_{\text{adv}}^t = \pi_{\omega}^{\text{adv}}(\Phi^t)$. According to the zero-sum game structure, the agent receives the reward $r^t = R_2(\Phi^t, a_{\text{agent}}^t, a_{\text{adv}}^t)$, while the adversary receives a reward of $-r^t$. Hence, we can say that the optimal value function of the two-player zero-sum game is given by maximizing the worst-case value function due to adversarial policies. As provided in [53], the following performance objective is considered in the adversarial game,

$$J(\pi_{\theta}^{\text{agent}}, \pi_{\omega}^{\text{adv}}) = \mathbb{E} \left[\sum_{t=1}^{\infty} \gamma^{t-1} r^t \mid \pi_{\theta}^{\text{agent}}, \pi_{\omega}^{\text{adv}}, \mathcal{M}_2 \right]. \quad (9)$$

where $\sum_{t=1}^{\infty} \gamma^{t-1} r^t$ is the random cumulative return. If we write, $J(\theta, \omega) = J(\pi_{\theta}^{\text{agent}}, \pi_{\omega}^{\text{adv}})$ the following objective has to be considered for analysis,

$$\max_{\theta \in \Theta} \min_{\omega \in \Omega} J(\theta, \omega). \quad (10)$$

In equation (11), J is nonconvex and nonconcave in both θ and ω . When a mixed strategy is applied to solve (11),

the optimal solution can be determined over the set of all probability distributions of Θ and Ω , as given by

$$\max_{p \in \mathcal{P}(\Theta)} \min_{q \in \mathcal{P}(\Omega)} f(p, q) := \mathbb{E}_{\theta \sim p} [\mathbb{E}_{\omega \sim q} [J(\theta, \omega)]] \quad (11)$$

The objective in (12) can be solved using the algorithm for finding the mixed-Nash equilibrium in generative adversarial networks (GANs) [54], as demonstrated for robust RL problems in [53]. In this action-robust RL scenario, the agent and adversarial policy networks can be viewed as the generator and discriminator networks in a GAN, respectively. Sampling-based methods are employed to derive the mixed-Nash equilibrium from the objective function in equation (12), as detailed in [54]. The solution methods for (12) has been provided in Appendix B which is similar to [12]. Although this formulation focuses on action-space perturbations, its outcomes generalize across uncertain environments. Robust agents trained under these conditions tend to exhibit more conservative and stable policies, which are resilient to shifts in the input distribution. This property makes the shared critic Q_{AR} a valuable expert baseline for adapting to observation-space adversarial attacks (e.g., GPS spoofing or state perturbations).

IV. ANTIFRAGILE LEARNING BY CURRICULUM GUIDED ADVERSARIAL DISTRIBUTIONAL ADAPTATION

A. Threat Model

1) *Simulated Adversary for Antifragile Adaptation:* To promote antifragility, we simulate a curriculum-based adversary during training that exposes the policy to increasingly perturbed state distributions. This simulated attacker is not designed to degrade performance but instead enables robust critic alignment and domain-level adaptation across adversarial intensities. Adversarial states are crafted via gradient-based perturbations using the policy's own loss gradients. A multi-step projected gradient ascent method is employed to maximize the policy loss within a norm-bounded region [55]:

$$\Phi_{n+1} = \Pi \left[\Phi_n + \frac{\varepsilon}{N_{\text{step}}} \cdot \text{sgn}(\nabla_{\Phi_n} \mathcal{L}_{\pi}) \right], \quad (12)$$

where ε is the total attack budget, $\text{sgn}(\cdot)$ is the sign function, and Π is the projection operator to ensure valid observation bounds. To reduce computational cost, we also use the single-step fast gradient sign method (FGSM) [56]:

$$\Phi_{n+1} = \Phi_n + \varepsilon \cdot \text{sgn}(\nabla_{\Phi_n} \mathcal{L}_{\pi}). \quad (13)$$

Since observations are normalized to $\mathcal{N}(0, 1)$, both (12) and (13) induce structured distributional shifts. However, FGSM is less effective under strong perturbations and may cause overfitting due to unstable gradients [57, 58]. To mitigate this, we incorporate ZeroGrad [59], which selectively nullifies unstable gradient components to improve robustness. Let $\delta_1, \delta_2, \dots, \delta_k$ represent k perturbations from different initial states. The shared sign set is defined as:

$$A = \{i \mid 1 \leq i \leq d, [\text{sgn}(\delta_1)]_i = [\text{sgn}(\delta_j)]_i \ \forall j \in \{2, \dots, k\}\}. \quad (14)$$

The adversarial curriculum gradually increases ε across training stages to simulate escalating threat levels. The overall

algorithm for adversarial state generation is provided in Algorithm 1 in Appendix C.

Remark 1. The ZeroGrad mechanism [59] used in the simulated adversarial curriculum regularizes the second derivative of the loss function by neutralizing fragile input gradients. This technique is inspired by prior work on robust gradient filtering in adversarial training regimes. To the best of our knowledge, this is the first application of ZeroGrad in the context of curriculum-based antifragile adaptation.

2) *Evaluation Against Unknown Adversary:* In the evaluation phase, we assess the trained policy under a high-capability attacker that persistently perturbs UAV observations at test time. This models real-world threats such as GPS spoofing or sensor tampering in safety-critical airspace.

Attacker Capabilities and Assumptions:

- **White-box access:** The adversary is assumed to reconstruct the policy via imitation learning (e.g., GAIL [18]), allowing computation of gradients $\nabla_{\Phi} \mathcal{L}_{\pi}$.
 - **Perturbation strategy:** Multi-step projected gradient descent (PGD) is used to iteratively generate adversarial observations within an L_{∞} -bounded ball.
 - **Spoofing simulation:** Structured perturbations are injected into geolocation features, simulating spoofed GPS or ADS-B interference.
 - **Temporal persistence:** Perturbations are applied at each decision step, mimicking continuous sensor compromise.
- Adversary Objective:* The attacker aims to:
- Increase divergence between clean and perturbed TD-error distributions.
 - Reduce cumulative reward and navigation efficiency.
 - Induce unsafe actions or elongated flight trajectories, potentially enabling UAV hijacking or conflict escalation.

This test-time threat model reflects practical vulnerabilities in UAV deployments within UTM systems. Given the use of unencrypted channels and external satellite signals, adversaries can realistically distort the UAV's perceived state, compromising airspace safety. Evaluating under this model allows us to validate the safety and antifragility of the proposed policy framework.

B. Curriculum Guided-Antifragile Adaptation Framework

Generally, predictive likelihood function is used to differentiate different task distributions for a batch of samples (X, Y) , following the methodological framework outlined in [60]. Specifically, if we consider $X = (\Phi^t, a^t)$, then the target $Y = r^t + \gamma Q_{\phi}(\Phi^{t+1}, \pi_{\theta}(\Phi^{t+1}))$. the likelihood $p_{\vartheta}(Y | X)$ parameterized by ϑ is given by,

$$\begin{aligned} p_{\vartheta}(Y | X) &= \prod_i \mathcal{N}(y_i, \hat{y}_i, \sigma^2), \\ &= \prod_i \mathcal{N}(r_i^t + \gamma Q_{\phi}(\Phi_i^{t+1}, \pi_{\theta}(\Phi_i^{t+1})); Q_{\phi}(\Phi_i^t, a_i^t), \sigma^2). \end{aligned} \quad (15)$$

In (15), σ refers to the standard deviation of the error distribution. The metric in (16) also represents the TD error for a particular state experience $(\Phi^t, a^t, \Phi^{t+1}, r^t)$. Similarly, for the state action pair (Φ_i^t, a_i^t) following the DDPG policy

π_{DDPG} , with the critic value function parameterized by ϕ given by Q_{ϕ} . The TD error is defined as,

$$\mathbf{TD}_{\Phi}^{\text{DDPG}} = \prod_i \mathcal{N}(r_i^t + \gamma Q(\Phi_i^{t+1}, \pi_{\text{DDPG}}(\Phi_i^{t+1})); Q(\Phi_i^t, a_i^t), \sigma^2). \quad (16)$$

Similarly, TD error $\mathbf{TD}_{\Phi_{\text{adv}}^{\varepsilon}}^{\text{AR}}$ for the action robust critic Q_{AR} with adversarial experience at time t , $\{\Phi_{\text{adv}}^{\varepsilon}, a_{\text{adv}}^{\varepsilon}, \Phi^{t+1}, r_{\text{adv}}^{\varepsilon}\}$ is given as,

$$\begin{aligned} \mathbf{TD}_{\Phi_{\text{adv}}^{\varepsilon}}^{\text{AR}} &= \prod_i \mathcal{N}\left(r_{\text{adv}_i}^{\varepsilon} + \gamma Q_{\text{AR}}(\Phi_i^{t+1}, (1 - \alpha) \cdot \pi_{\theta}^{\text{agent}}(\Phi_i^{t+1}) \right. \\ &\quad \left. + \alpha \cdot \pi_{\omega}^{\text{adv}}(\Phi_i^{t+1})); Q_{\text{AR}}(\Phi_{\text{adv}_i}^{\varepsilon}, a_{\text{adv}_i}^{\varepsilon}), \sigma^2\right). \end{aligned} \quad (17)$$

In order to analyze the TD error, we need to consider the following assumptions.

Assumption 1. [61] The reward function decreases under stronger adversarial perturbation, $r^{\varepsilon_{k+1}} - r^{\varepsilon_k} \leq 0$.

Assumption 1 is justified since the adversarial perturbations distort the UAV's perceived state Φ_{ε} , which causes incorrect estimation of the relative position of the obstacles or possibly riskier maneuvers or unnecessary avoidance. This leads to greater likelihood of entering threat zones or faulty replanning. In consequence lower rewards can be obtained, as described in the previous section.

Assumption 2. [62] Considering Lipschitz rewards and transition, with the smooth system dynamics and response, the value function under optimal policy π^* is Lipschitz continuous with respect to adversarial state Φ_{ε_k} and the transition state Φ'_{ε_k} , given as,

$$|Q_k^{\pi^*}(\Phi_{\varepsilon_k}) - Q_k^{\pi^*}(\Phi'_{\varepsilon_k})| \leq L_Q d(\Phi_{\varepsilon_k}, \Phi'_{\varepsilon_k}). \quad (18)$$

Considering the state evolution of UAV kinematics and environmental response like the obstacle motion are governed by smooth differentiable functions, hence small changes in the input state results in bounded changes in future state transition and value estimates. This validates the usage of assumption 2. Hence, consider the above assumption, with the Lipschitz continuity of the reward function we can write,

$$|r^{\varepsilon_k} - r^{\varepsilon_{k+1}}| \leq -L_r d(\Phi_{\varepsilon_k}, \Phi_{\varepsilon_{k+1}}) \leq 0. \quad (19)$$

Based on the definition of TD-error, the catastrophic forgetting is quantified as the 1-Wasserstein distance $\mathcal{W}_1(\cdot)$ between the two distributions for the adversarial state $\Phi_{\text{adv}}^{\varepsilon}$ shown as,

$$f_{\pi}^{\varepsilon} = \inf_{\pi \in \Pi(\mathbf{TD}_{\text{DDPG}}, \mathbf{TD}_{\pi}^{\varepsilon})} \mathbb{E}_{(x,y) \sim \pi} [\|\mathbf{TD}_{\text{DDPG}} - \mathbf{TD}_{\pi}^{\varepsilon}\|_1]. \quad (20)$$

The following theorem suggests a monotonic increase in the catastrophic forgetting with adversarial strength.

Theorem 1. Let π be a fixed and non-adaptive policy. Let Φ_{ε} denote the adversarially perturbed observation of a nominal UAV state Φ , with perturbation strength ε . Suppose the TD-error distributions $\mathbf{TD}_{\pi}^{\varepsilon}$ are induced by policy π under increasing perturbation levels $\varepsilon_1 < \varepsilon_2$, and the catastrophic forgetting value is defined as in (20). Assume that the Lipschitz continuity assumptions given in Assumption 1 and Assumption

2 for the critic, and reward functions are satisfied. Then we have

$$f_{\pi}^{\varepsilon_1} < f_{\pi}^{\varepsilon_2}. \quad (21)$$

Proof: Let us consider the next state given by Φ^+ , which it transits from initial state Φ . Similarly it transits to $\Phi^{\varepsilon,+}$ from the adversarial state Φ^{ε} . The expected TD-error under perturbation ε is given by:

$$\mathbf{TD}_{\pi}^{\varepsilon} := r^{\varepsilon} + \gamma Q^{\pi}(\Phi^{\varepsilon,+}, \pi(\Phi^{\varepsilon,+})) - Q^{\pi}(\Phi^{\varepsilon}, \pi(\Phi^{\varepsilon})), \quad (22)$$

and the nominal TD-error under clean state Φ be:

$$\mathbf{TD}_{\pi}^0 := r^0 + \gamma Q^{\pi}(\Phi^+, \pi(\Phi^+)) - Q^{\pi}(\Phi, \pi(\Phi)). \quad (23)$$

We analyze the difference of the above TD errors as:

$$\begin{aligned} |\mathbf{TD}_{\pi}^{\varepsilon} - \mathbf{TD}_{\pi}^0| &\leq |r^{\varepsilon} - r^0| \\ &+ \gamma |Q^{\pi}(\Phi^{\varepsilon,+}, \pi(\Phi^{\varepsilon,+})) - Q^{\pi}(\Phi^+, \pi(\Phi^+))| \\ &+ |Q^{\pi}(\Phi^{\varepsilon}, \pi(\Phi^{\varepsilon})) - Q^{\pi}(\Phi, \pi(\Phi))|. \end{aligned} \quad (24)$$

Considering the Lipschitz continuity in rewards, critic and policy function, the following relations can be used.

$$\begin{aligned} |Q^{\pi}(\Phi^{\varepsilon}, \pi(\Phi^{\varepsilon})) - Q^{\pi}(\Phi, \pi(\Phi))| &\leq L_Q(1 + L_{\pi}) \|\Phi^{\varepsilon} - \Phi\|, \\ |Q^{\pi}(\Phi^{\varepsilon,+}, \pi(\Phi^{\varepsilon,+})) - Q^{\pi}(\Phi^+, \pi(\Phi^+))| &\leq L_Q(1 + L_{\pi}) \|\Phi^{\varepsilon,+} - \Phi^+\|. \end{aligned} \quad (25)$$

Therefore, we can write:

$$\begin{aligned} |\mathbf{TD}_{\pi}^{\varepsilon} - \mathbf{TD}_{\pi}^0| &\leq (L_r + L_Q(1 + L_{\pi})) \|\Phi^{\varepsilon} - \Phi\| \\ &+ \gamma L_Q(1 + L_{\pi}) \|\Phi^{\varepsilon,+} - \Phi^+\|. \end{aligned} \quad (26)$$

Since $\varepsilon_2 > \varepsilon_1$ implies:

$$\|\Phi^{\varepsilon_2} - \Phi\| > \|\Phi^{\varepsilon_1} - \Phi\|, \quad \|\Phi^{\varepsilon_2,+} - \Phi^+\| > \|\Phi^{\varepsilon_1,+} - \Phi^+\|,$$

we conclude:

$$|\delta^{\varepsilon_2} - \delta^0| > |\delta^{\varepsilon_1} - \delta^0|. \quad (27)$$

Taking expectation over all states Φ , we obtain:

$$f_{\pi}^{\varepsilon_1} = \mathbb{E} [|\delta^{\varepsilon_1} - \delta^0|] < \mathbb{E} [|\delta^{\varepsilon_2} - \delta^0|] = f_{\pi}^{\varepsilon_2}. \quad (28)$$

As established in Theorem 1, the fragile behavior of non-adaptive policies is characterized where performance deteriorates progressively under stronger perturbations. To counteract this degradation and promote antifragility, the policy must adapt such that the rate of forgetting is stabilized or reduced as perturbations intensify. In other words, an antifragile policy does not merely resist adversarial effects, but leverages domain-level adaptation to suppress the increase in catastrophic forgetting, thereby improving or maintaining temporal difference alignment across adversarial environments. The formal definition of an antifragile policy is provided below.

Definition 1 (Antifragile Policy under Adversarial Perturbations). Let π^{af} be a RL policy trained using domain-adaptive mechanisms (e.g., expert critics or adversarial curriculum). Then π^{af} is said to be antifragile if, for increasing adversarial

perturbation levels $\varepsilon_1 < \varepsilon_2 < \dots < \varepsilon_K$, the corresponding catastrophic forgetting values

$$f_{\pi^{\text{af}}}^{\varepsilon_k} = \inf_{\gamma \in \Pi(\mathbf{TD}_{\text{DDPG}}, \mathbf{TD}_{\pi^{\text{af}}}^{\varepsilon_k})} \mathbb{E}_{(x,y) \sim \gamma} [\|x - y\|_1]$$

are bounded and non-increasing up to a constant $\delta > 0$, such that:

$$|f_{\pi^{\text{af}}}^{\varepsilon_{k+1}} - f_{\pi^{\text{af}}}^{\varepsilon_k}| \leq \delta, \quad \forall k \in \{1, \dots, K-1\}, \quad (29)$$

and

$$f_{\pi^{\text{af}}}^{\varepsilon_k} < f_{\pi}^{\varepsilon_k}, \quad (30)$$

where π is a non-adaptive baseline policy (e.g., DDPG or robust RL) evaluated under the same perturbations.

In order to obtain the condition in (29), we use the following lemmas to derive the learning procedure. If we consider P_k the distribution that governs the transition probability for the adversarial state ε_k , i.e. Φ_{ε_k} to Φ'_{ε_k} , then we consider the relation as per the following lemma.

Lemma 1. The change in expected value function under different adversarial perturbations is controlled by Wasserstein 1-distance. It is expressed as,

$$\begin{aligned} & \left| \mathbb{E}_{\Phi'_{\varepsilon_{k+1}} \sim P_{k+1}} [Q_{k+1}^{\pi^*}(\Phi'_{\varepsilon_{k+1}})] - \mathbb{E}_{\Phi'_{\varepsilon_k} \sim P_k} [Q_k^{\pi^*}(\Phi'_{\varepsilon_k})] \right| \\ & \leq L_Q \mathcal{W}_1(P_{k+1}, P_k). \end{aligned} \quad (31)$$

Proof: Proof in Appendix D.I. ■

Lemma 1 states that small shifts in the distribution of the transitioned state, with incremental perturbation leads to bounded and stable change in the value distributions. Now we consider, the change in the value distributions with the adversarial state instead of transitioned state as follows.

Lemma 2. The optimal value function does not change abruptly between adversarial perturbation levels

$$|Q_{k+1}^{\pi^*}(\Phi_{\varepsilon_{k+1}}) - Q_k^{\pi^*}(\Phi_{\varepsilon_k})| \leq L_Q d(\Phi_{\varepsilon_{k+1}}, \Phi_{\varepsilon_k}). \quad (32)$$

Proof: Proof in Appendix D.II. ■

Having established the relationship between the value function and the perturbed next-state distribution, we now investigate how the transition probability distribution itself evolves as the level of adversarial perturbation increases. This relationship is formalized in the following lemma.

Lemma 3. If $\mathcal{W}_1(\cdot)$ represents the 1-Wasserstein distance between two probability distributions P_k and P_{k+1} over the state space of \mathcal{S} , then we can consider for the states $\Phi'_{\varepsilon_k} \sim P_k$, $\Phi'_{\varepsilon_{k+1}} \sim P_{k+1}$, then we can consider,

$$\mathcal{W}_1(P_{k+1}, P_k) \leq \mathcal{W}_1(\mathbf{TD}_{k+1}^{\pi^*}(\varepsilon_{k+1}), \mathbf{TD}_k^{\pi^*}(\varepsilon_k)). \quad (33)$$

Proof: Proof as per Appendix D.III. ■

Lemma 4. If we consider the adversarial states Φ_{ε_k} and $\Phi_{\varepsilon_{k+1}}$, with $\varepsilon_{k+1} > \varepsilon_k$ then the distance between the adversarial states $d(\Phi_{\varepsilon_k}, \Phi_{\varepsilon_{k+1}})$ is constrained by the distributional distance of the transition distribution P_k and P_{k+1} , which is given by,

$$d(\Phi_{\varepsilon_k}, \Phi_{\varepsilon_{k+1}}) \leq \mathcal{W}_1(P_k, P_{k+1}). \quad (34)$$

Proof: Proof given in Appendix D.IV ■

Based on the above assumptions, and lemmas now the following theorem is provided which adapts the robust policy against incremental adversarial states to induce antifragility.

Theorem 2. *Considering the Lipschitz assumption for the reward and the value function in Assumption 1 and 2, while considering m to be a problem specific positive constant, for any consecutive stages $k, k+1 \in [K]$, the corresponding optimal policies π^k and π^{k+1} satisfy the following relationship with respect to the TD-error,*

$$\begin{aligned} & \mathbb{E} \left[\mathbf{TD}^{\pi_{k+1}^*}(\epsilon_{k+1}) - \mathbf{TD}^{\pi_k^*}(\epsilon_{k+1}) \right] \\ & \leq m \mathcal{W}_1 \left(\mathbf{TD}^{\pi_{k+1}^*}(\epsilon_{k+1}), \mathbf{TD}^{\pi_k^*}(\epsilon_k) \right). \end{aligned} \quad (35)$$

Proof: If we consider for an adversarial perturbed state under the attack strength ϵ_1 as $\Phi_{\text{adv}}^{\epsilon_1}$, then for adversarial strength $\epsilon_2 > \epsilon_1$, we take the difference between the expectation of the TD error as,

$$\begin{aligned} & \mathbb{E} \left[\mathbf{TD}^{\pi_{k+1}^*}(\epsilon_{k+1}) - \mathbf{TD}^{\pi_k^*}(\epsilon_k) \right] \\ & = r^{\epsilon_{k+1}} - r^{\epsilon_k} + \gamma \mathbb{E}_{\Phi'_{\epsilon_{k+1}} \sim P_{k+1}} \left[Q_{k+1}^{\pi^*}(\Phi'_{\epsilon_{k+1}}) \right] - Q_{k+1}^{\pi^*}(\Phi_{\epsilon_{k+1}}) \\ & - \left(\gamma \mathbb{E}_{\Phi'_{\epsilon_k} \sim P_{k+1}} \left[Q_k^{\pi^*}(\Phi'_{\epsilon_k}) \right] - Q_k^{\pi^*}(\Phi_{\epsilon_k}) \right) \\ & = (r^{\epsilon_{k+1}} - r^{\epsilon_k}) + \gamma \mathbb{E}_{\Phi'_{\epsilon_{k+1}} \sim P_{k+1}} \left[Q_{k+1}^{\pi^*}(\Phi'_{\epsilon_{k+1}}) \right] \\ & - \gamma \mathbb{E}_{\Phi'_{\epsilon_k} \sim P_k} \left[Q_k^{\pi^*}(\Phi'_{\epsilon_k}) \right] - \left(Q_{k+1}^{\pi^*}(\Phi_{\epsilon_{k+1}}) - Q_k^{\pi^*}(\Phi_{\epsilon_k}) \right). \end{aligned} \quad (36)$$

If we consider the Assumption 1 and 2 and Lemma 1 and 2 and apply the bounds as per in (36), we obtain,

$$\begin{aligned} & \mathbb{E} \left[\mathbf{TD}^{\pi_{k+1}^*}(\epsilon_{k+1}) - \mathbf{TD}^{\pi_k^*}(\epsilon_k) \right] \leq \\ & \gamma L_V \mathcal{W}_1(P_{k+1}, P_k) + L_V d(\Phi_{\epsilon_{k+1}}, \Phi_{\epsilon_k}). \end{aligned} \quad (37)$$

If we use the relation in lemma 4,

$$d(\Phi_{\epsilon_{k+1}}, \Phi_{\epsilon_k}) \leq \mathcal{W}_1(P_{k+1}, P_k), \quad (38)$$

We obtain the following relation,

$$\begin{aligned} & \mathbb{E} \left[\left| \mathbf{TD}^{\pi_{k+1}^*}(\epsilon_{k+1}) - \mathbf{TD}^{\pi_k^*}(\epsilon_k) \right| \right] \leq \\ & L_V (1 + \gamma) \mathcal{W}_1(P_{k+1}, P_k). \end{aligned} \quad (39)$$

Now, we per the lemma 3, the distributional distance between the state distributions P_k and P_{k+1} , which differ in Wasserstein distance based on ϵ_k and ϵ_{k+1} , as

$$\mathcal{W}_1(P_{k+1}, P_k) \leq \mathcal{W}_1(\mathbf{TD}^{\pi_{k+1}^*}(\epsilon_{k+1}), \mathbf{TD}^{\pi_k^*}(\epsilon_k)). \quad (40)$$

Hence, using the relation of the distance between the state distribution in lemma 3, the final relation becomes,

$$\begin{aligned} & \mathbb{E} \left[\left| \mathbf{TD}^{\pi_{k+1}^*}(\epsilon_{k+1}) - \mathbf{TD}^{\pi_k^*}(\epsilon_k) \right| \right] \leq \\ & m \mathcal{W}_1 \left(\mathbf{TD}^{\pi_{k+1}^*}(\epsilon_{k+1}), \mathbf{TD}^{\pi_k^*}(\epsilon_k) \right). \end{aligned} \quad (41)$$

Remark 2. *This behavior is enabled by the expert-guided domain adaptation strategy, which contracts the temporal difference (TD) error variation between adjacent perturbation levels. As shown in Theorem 2, if the Wasserstein distance*

between TD distributions across ϵ_k and ϵ_{k+1} is bounded, then the TD-error shift is similarly bounded:

$$\left| \mathbf{TD}^{\pi_{k+1}^*}(\epsilon_{k+1}) - \mathbf{TD}^{\pi_k^*}(\epsilon_k) \right| \leq m \cdot \mathcal{W}_1 \left(\mathbf{TD}^{\pi_{k+1}^*}(\epsilon_{k+1}), \mathbf{TD}^{\pi_k^*}(\epsilon_k) \right), \quad (42)$$

for a constant $m > 0$, under Lipschitz continuity assumptions. This contractive property stabilizes catastrophic forgetting, thus satisfying Definition 1.

V. RESULTS AND DISCUSSION

A. Numerical Simulations

The software implementation of the deep deterministic policy gradient algorithm (DDPG) for UAV navigation and deconfliction in environments with dynamic 3D obstacles was carried out as described in [63]. During the training phase, the initial position of the UAV was randomly generated with a mean vector of approximately (0, 2, 5) and a variance ranging from 0 to 1, while the target destination was set consistently at (10, 10, 5.5). To ensure realistic maneuverability, kinematic constraints were imposed, including a maximum ascent angle of $5\pi/9$ and a maximum descent angle of $-15\pi/36$. Furthermore, a safety buffer was implemented by enforcing a protective radius of 1.5 units around the UAV to mitigate collision risks. The dynamic obstacle used during training adhered to a predefined trajectory restricted to the xy plane, governed by the following equation.

$$\begin{aligned} x_{\text{obs}}(t) &= x_{\text{obs}}(t-1) + 2 \cos(t), \\ y_{\text{obs}}(t) &= y_{\text{obs}}(t-1) + 2 \sin(t). \end{aligned} \quad (43)$$

The reward function calculates the conflict penalty by augmenting the UAV's radius with an additional buffer of 0.4 units.

B. Results using Action Robust Reinforcement Learning

As illustrated in Fig. 3, the episodic rewards are plotted against the training episodes for action-robust RL with $\alpha = 0.1, 0.2, 0.3, 0.4$. It is evident that as the value of α increases, the episodic rewards exhibit a noticeable decline accompanied by increased uncertainty, particularly during the exploitation phase. A detailed examination of the reward distributions, as shown in Fig. 4, reveals that increasing α shifts the reward distribution to the left, while also increasing its variance. Further analysis of forgetting values f_{π}^{ϵ} for action-robust RL with varying attack strengths ϵ , depicted in Figure 5 under PGD attack described in (12) conducted in 10 steps. As evident in Theorem 1, we observe an increase in the forgetting value with the increase in ϵ . The forgetting value for vanilla DDPG is consistently higher than that of action-robust RL. This underscores the efficacy of robust learning in mitigating catastrophic forgetting compared to standard RL methods. However, for $\alpha = 0.4$, the forgetting value f_{π}^{ϵ} becomes comparable to that of the vanilla RL under significant distributional changes in the observation space (i.e. $\epsilon > 3.0$). In particular, the forgetting values of action-robust policies remain significantly lower for $\epsilon > 3.0$, with reduced uncertainty across a diverse range of adversarial samples. As we observe in Figure 5, the forgetting value is considerably lower for $\epsilon < 2.0$, hence the adaptation strategy is considered for antifragility for $\epsilon > 2.0$.

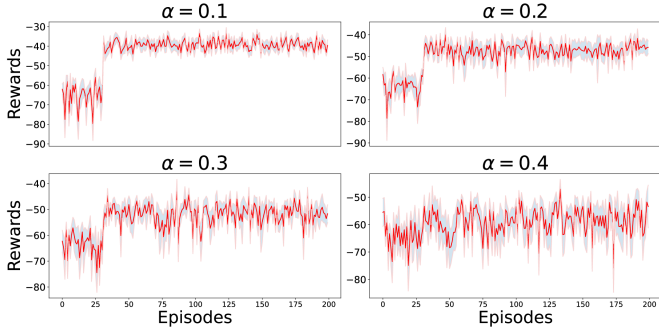


Fig. 3. The mean and uncertainty of the convergence episodic reward plot for action robust RL with different α when run with 10 Monte Carlo runs.

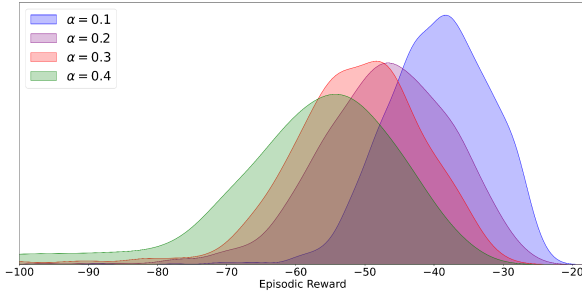


Fig. 4. Density plot of the converged rewards from previous 100 episodes from different α from action robust RL algorithms over 10 Monte Carlo runs.

C. Distributional Adaptation

The action-robust RL model with $\alpha = 0.1$ demonstrates the least catastrophic forgetting among robust frameworks, making it the preferred choice for adapting agents and adversarial policies against adversarial samples of increasing strength. These pre-trained policies are adapted following the procedures outlined in Algorithm 3, utilizing adversarial samples generated by Algorithm 1. The convergence characteristics for the algorithm governed by Theorem 2, is shown in Figure 6. As we observe that the algorithm converges at $\varepsilon = 5.0$, however in order to ensure generalizability against unseen attacks, we consider the test time model upto $\varepsilon = 4.0$. To evaluate the forgetting value f_{π}^{ε} , we compare the antifragile RL agent and adversarial policies under PGD attacks with

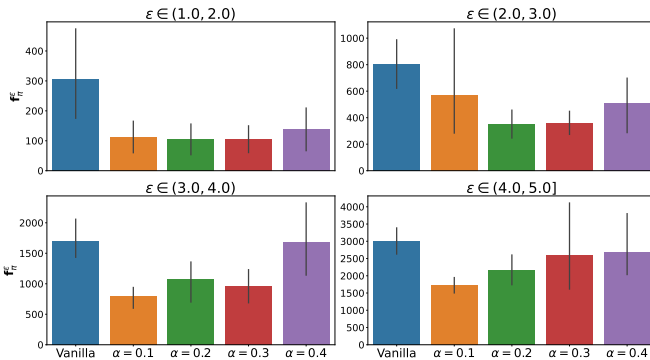


Fig. 5. Forgetting value f_{π}^{ε} of vanilla and action robust RL with different α under PGD attack when the value of ε is varied from 1.0 to 5.0.

strengths varying from $[1.0, 5.0]$ conducted in 10 steps. The forgetting value f_{π}^{ε} of the antifragile policies is consistently lower than that of the action robust framework with $\alpha = 0.1$, the effect being particularly significant for $\varepsilon \in (2.0, 3.0)$ and $\varepsilon \in (4.0, 5.0]$. Using increments of $\Delta\varepsilon = 0.25$, four distinct forgetting values are calculated, whose means and standard deviations are depicted in Figure 7. In particular, the domain adaptation framework shows a relative decrease in the mean and standard deviation of f_{π}^{ε} compared to the robust case with $\alpha = 0.1$.

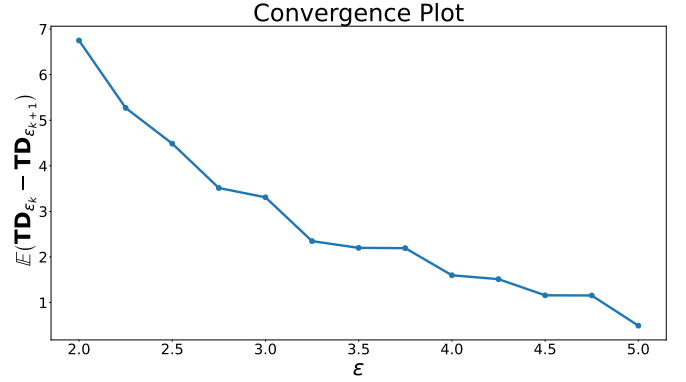


Fig. 6. Convergence plot of the value distribution bound with the increase in ε to ensure antifragile adaptation.

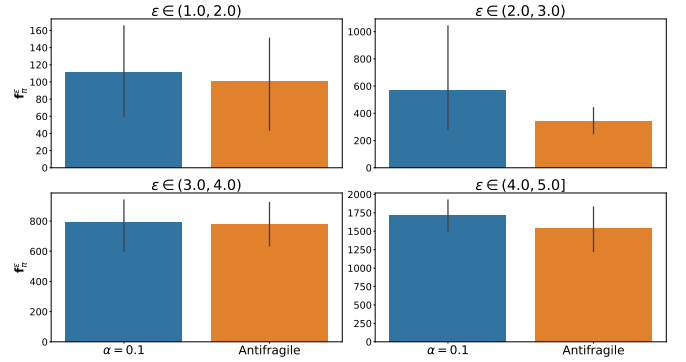


Fig. 7. Comparing the catastrophic forgetting value for antifragile with the robust framework for different intensities of adversarial attacks.

D. Benchmarking against Unknown Attacks

The antifragile mechanism is compared against the benchmarking robust and adversarial meta learning algorithms as outlined in Appendix (E). As detailed in Section IV-A2, the proposed antifragile framework is evaluated against previously unseen adversarial conditions, including multi-step (PGD) attacks and GPS spoofing. The PGD attack shares fundamental characteristics with ZeroGrad approach for adversarial states in that both leverage policy gradients to generate adversarial samples; however, PGD performs iterative perturbation updates, making it significantly more potent and capable of inducing severe policy degradation. In contrast, the spoofing attack

TABLE I
THE MEAN REWARD OF THE VANILLA DDPG, NR-MDP, PR-MDP, SA-MDP, ADVERSARIAL META LEARNING AND ANTIFRAGILE ALGORITHMS ALONG WITH STANDARD DEVIATIONS FOR DIFFERENT ADVERSARIAL AND SPOOFING ATTACKS

Models	PGD l_∞ attack $\epsilon = 4.0$	PGD l_∞ attack $\epsilon = 5.0$	Spoofing Attack
Vanilla DDPG	-52.90 \pm 12.44	-50.56 \pm 9.36	-71.22 \pm 8.29
NR-MDP [23]	-89.01 \pm 51.02	-73.16 \pm 20.15	-307.1 \pm 51.32
PR-MDP [23]	-74.27 \pm 23.07	-72.54 \pm 22.44	-248.0 \pm 39.28
SA-MDP [22]	-55.71 \pm 14.37	-54.35 \pm 12.97	-363.09 \pm 55.14
Adversarial Meta [64]	-59.01 \pm 10.18	-59.91 \pm 12.22	-327.76 \pm 60.32
Antifragile	-49.36 \pm 10.66	-47.80 \pm 8.86	-60.05 \pm 11.42

introduces a persistent positional bias to the UAV's geolocation, representing a structurally different and entirely unknown threat. This bias causes consistent deviations from the planned trajectory, simulating real-world GPS manipulation scenarios in unmanned airspace.

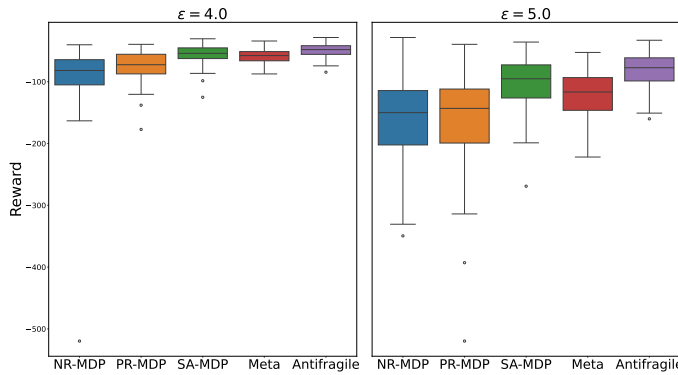


Fig. 8. Comparing the testing reward of antifragile policy with the existing robust and adversarial meta RL policies under l_∞ PGD attack for $\epsilon = 4.0, 5.0$.

1) Multi-Step Adversarial Attacks with Multiple Obstacles:

We now analyze a scenario involving multiple dynamic obstacles, specifically eight obstacles that follow predetermined trajectories. Furthermore, we apply the adversarial PGD attack with $N_{\text{step}} = 50$, which represents a significantly more robust adversarial perturbation compared to the attack considered previously. The ownship UAV identifies the nearest obstacle and executes maneuvers accordingly. To evaluate performance under stronger adversarial conditions, a PGD attack is applied over 50 steps. The overall performance of the antifragile RL framework is compared with different robust approaches like policy iteration using NR-MDP, PR-MDP, convex relaxation using state adversarial MDP (SA-MDP) and meta adversarial RL approach as per Figure 8. As illustrated in Figure 8, the antifragile policy achieves the highest cumulative reward under PGD-based adversarial perturbations, indicating successful adaptation and robust alignment of value estimates across varying perturbed domains. This performance highlights the antifragile property of the policy—demonstrating not only resistance to adversarial influence but also the ability to exploit such perturbations to preserve optimal behavior. While both Meta-RL and SA-MDP baselines exhibit improved resilience due to prior exposure to adversarial distributions

during training, the Meta policy slightly outperforms SA-MDP, potentially due to its stronger task generalization capability. However, despite reduced conflict rates observed during navigation—consistent with prior findings in [12]—both approaches incur lower overall rewards compared to the antifragile policy. This disparity can be attributed to their inability to account for trajectory length efficiency, resulting in suboptimal path planning under adversarial conditions. NR-MDP, trained without adversarial considerations, and PR-MDP, which uses static robustness formulations, fail to retain performance under dynamic perturbation, validating the findings from Theorem 1 regarding catastrophic forgetting in non-adaptive agents. These results under PGD attacks validate the theoretical bounds for antifragile adaptation and demonstrate the policy's resilience to high-frequency gradient-based perturbations. We now examine the performance under a structurally different, persistent threat: GPS spoofing.

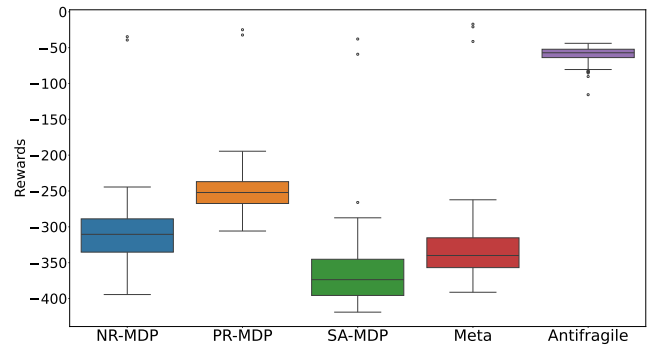


Fig. 9. Comparing the testing reward of antifragile policy with the existing robust and adversarial meta RL policies under spoofing attack.

2) *Spoofing Attack*: In the GPS spoofing scenario, a constant positional bias of 0.05 units was applied to the UAV's position vector at every timestep, following the setup described in [12]. We assume the UAV possesses sufficient energy and control authority to complete its mission despite the induced drift, thereby enabling a fair evaluation of policy robustness. Unlike PGD-based attacks, which are gradient-driven and episodically localized, the spoofing attack introduces a persistent, structured shift in observation space. As reported in Table I, this results in a significant decline in average cumulative reward across all evaluated algorithms. The observed degradation suggests that such spoofing strategies can induce substantial deviations in planned trajectories, increasing the risk of misnavigation or potential hijacking. Figure 9 illustrates that the antifragile policy consistently achieves the highest average reward under spoofing conditions. This performance reflects its capacity to adaptively stabilize value estimates across distorted observational inputs, thereby mitigating catastrophic forgetting. Meta-RL and SA-MDP policies demonstrate improved robustness over nominal (NR-MDP) and statically robust (PR-MDP) baselines, likely due to their exposure to adversarial domains during training. However, their inability to explicitly align value functions under distributional shifts results in significantly lower performance compared to the antifragile approach. The superior reward retention of the antifragile policy is attributed to its expert-

guided critic alignment mechanism, which dynamically adapts to increasing perturbation levels. Unlike static regularization-based methods, this framework actively suppresses forgetting by reinforcing value consistency across perturbed domains. Consequently, it maintains safe, high-reward trajectories even under severe adversarial influence. These empirical results validate the theoretical predictions outlined in Theorem 1, and demonstrate the practical advantages of antifragile RL in secure autonomous decision-making under observation-space attacks.

E. Ablation Study: Impact of Safe Navigation

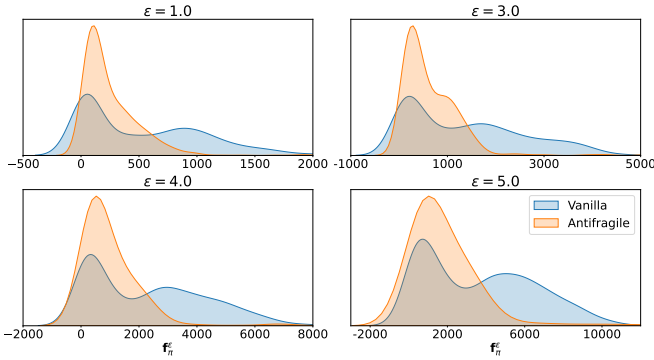


Fig. 10. Comparing the forgetting value for the vanilla DDPG and antifragile framework with different intensities of adversarial attacks.

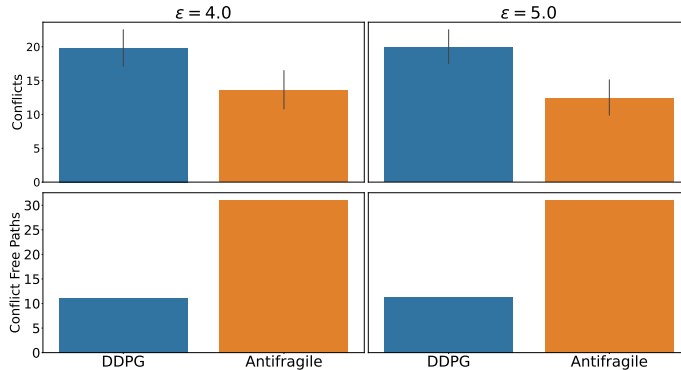


Fig. 11. Comparing the safety performance of antifragile policy with the DDPG policy under l_∞ PGD attack for $\epsilon = 4.0, 5.0$.

As part of the ablation study, we compare the proposed antifragile policy against the standard DDPG baseline to assess safety-critical performance under adversarial perturbations. As shown in Figure 10, the DDPG baseline experiences increased catastrophic forgetting under strong adversarial conditions, with its (TD) error distribution exhibiting a multi-modal pattern. This instability reflects the policy's inability to maintain consistent value estimates across perturbed inputs. In contrast, the antifragile policy demonstrates a more stable learning process, preserving a unimodal TD-error distribution that indicates reduced forgetting and improved critic alignment. Based on the reduction of catastrophic forgetting, the proposed

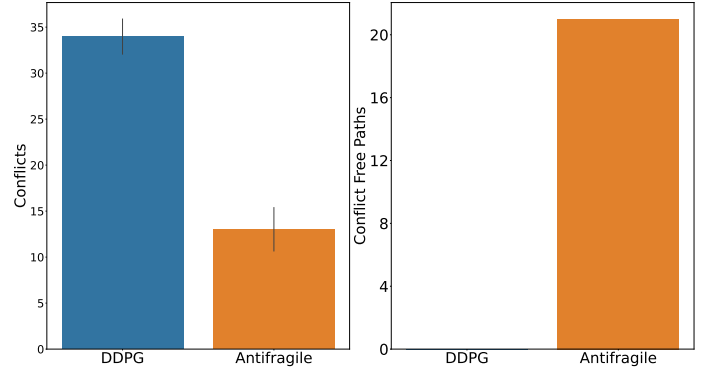


Fig. 12. Comparing the safety performance of antifragile policy with the DDPG policy under spoofing attack.

antifragile policy exhibits a markedly lower number of conflict events compared to the DDPG baseline as shown in Figure 11, underscoring its enhanced capacity to operate safely in adversarial environments. This aligns with the intended objective of minimizing exposure to high-risk, repulsive-force zones. Furthermore, the number of successful, conflict-free trajectory completions is substantially higher for the antifragile policy, indicating improved generalization and decision reliability under adversarial perturbations. These findings confirm that in the absence of antifragile adaptation, standard DDPG agents are unable to preserve safety guarantees when exposed to perturbed observations. The safety performance reinforces the importance of adaptive critic alignment mechanisms, as formalized in Theorem 2 and Definition 1. Under GPS spoofing attacks, as illustrated in Figure 12, the antifragile policy again demonstrates a significant safety advantage over the DDPG baseline. While DDPG experiences frequent conflict events and fails to maintain trajectory stability in the presence of persistent positional bias, the antifragile policy consistently avoids unsafe regions and successfully completes a greater proportion of conflict-free paths.

VI. CONCLUSION

This paper presents a theoretically grounded and empirically validated antifragile RL framework for secure UAV navigation under adversarial observation-space attacks. We formally define the concepts of fragility and antifragility in the context of RL by introducing a distributional perspective on catastrophic forgetting, quantified via the Wasserstein distance between temporal-difference (TD) error distributions. A key theoretical contribution includes deriving provable bounds on TD-error divergence under adversarial perturbations, and demonstrating that non-adaptive agents experience monotonic increases in forgetting, while antifragile policies ensure bounded adaptation. We benchmark our antifragile policy against state-of-the-art baselines, including NR-MDP, PR-MDP, SA-MDP, and adversarial meta-learning, across strong projected gradient descent (PGD) and GPS spoofing attacks. We summarize the contribution and the results as follows:

- **Theoretical formulation of fragility and antifragility:** Catastrophic forgetting is formally defined using the

Wasserstein-1 distance between TD-error distributions, enabling a principled distinction between fragile and antifragile policies under adversarial perturbations.

- **Provable bounds for antifragile adaptation:** Theoretical guarantees are established showing that antifragile policies maintain bounded TD-error divergence as adversarial strength increases, supported by Lemmas and Theorem 2.
- **Superior reward performance under strong attacks:** The antifragile policy consistently outperforms NR-MDP, PR-MDP, SA-MDP, and Meta-RL baselines under multi-step PGD and GPS spoofing attacks, achieving higher cumulative reward and demonstrating effective adaptation.
- **Improved safety in ablation studies:** Compared to the DDPG baseline, the antifragile policy exhibits fewer conflict events in adversarial scenarios and higher number of conflict-free trajectory completions.

This research can be extended by incorporating multi-agent antifragile learning for cooperative UAV swarms operating under decentralized adversarial observation-space attacks and dynamic threat landscapes.

REFERENCES

- [1] N. N. Taleb, *Antifragile: Things that gain from disorder*. Random House Trade Paperbacks, 2014, vol. 3.
- [2] C. Axenie *et al.*, “Antifragility in complex dynamical systems,” *npj Complexity*, vol. 1, no. 1, p. 12, 2024.
- [3] A. Perrusquía, W. Guo, B. Fraser, and Z. Wei, “Uncovering drone intentions using control physics informed machine learning,” *Communications Engineering*, vol. 3, no. 1, p. 36, 2024.
- [4] A. Tsourdos, B. White, and M. Shanmugavel, *Cooperative path planning of unmanned aerial vehicles*. John Wiley & Sons, 2010.
- [5] S. Aggarwal and N. Kumar, “Path planning techniques for unmanned aerial vehicles: A review, solutions, and challenges,” *Computer communications*, vol. 149, pp. 270–299, 2020.
- [6] X. Ye, F. Song, Z. Zhang, and Q. Zeng, “A review of small uav navigation system based on multi-source sensor fusion,” *IEEE Sensors Journal*, 2023.
- [7] N. Gyagenda, J. V. Hatilima, H. Roth, and V. Zhmud, “A review of gnss-independent uav navigation techniques,” *Robotics and Autonomous Systems*, vol. 152, p. 104 069, 2022.
- [8] R. Papa, I. Cardei, and M. Cardei, “Generalized path planning for utm systems with a space-time graph,” *IEEE open journal of intelligent transportation systems*, vol. 3, pp. 351–368, 2022.
- [9] A. Hamissi and A. Dhraief, “A survey on the unmanned aircraft system traffic management,” *ACM Computing Surveys*, vol. 56, no. 3, pp. 1–37, 2023.
- [10] Y. Kim, J.-Y. Jo, and S. Lee, “Ads-b vulnerabilities and a security solution with a timestamp,” *IEEE Aerospace and Electronic Systems Magazine*, vol. 32, no. 11, pp. 52–61, 2017.
- [11] X. Ying, J. Mazer, G. Bernieri, M. Conti, L. Bushnell, and R. Poovendran, “Detecting ads-b spoofing attacks using deep neural networks,” in *2019 IEEE conference on communications and network security (CNS)*, IEEE, 2019, pp. 187–195.
- [12] D. K. Panda and W. Guo, “Action robust reinforcement learning for air mobility deconfliction against conflict induced spoofing,” *IEEE Transactions on Intelligent Transportation Systems*, vol. 25, no. 12, pp. 21 343–21 355, 2024.
- [13] M. Leonardi, E. Piracci, and G. Galati, “Ads-b jamming mitigation: A solution based on a multichannel receiver,” *IEEE Aerospace and Electronic Systems Magazine*, vol. 32, no. 11, pp. 44–51, 2017.
- [14] Y. Lin and S. Saripalli, “Sampling-based path planning for uav collision avoidance,” *IEEE Transactions on Intelligent Transportation Systems*, vol. 18, no. 11, pp. 3179–3192, 2017.
- [15] F. Gavilan, R. Vazquez, and E. F. Camacho, “An iterative model predictive control algorithm for uav guidance,” *IEEE Transactions on Aerospace and Electronic Systems*, vol. 51, no. 3, pp. 2406–2419, 2015.
- [16] A. B. Nassif, M. A. Talib, Q. Nasir, H. Albadani, and F. M. Dakalbab, “Machine learning for cloud security: A systematic review,” *IEEE Access*, vol. 9, pp. 20 717–20 735, 2021.
- [17] Y. Kim, K. Cho, and S. Kim, “Challenges in drone firmware analyses of drone firmware and its solutions,” *IEEE Access*, 2024.
- [18] J. Ho and S. Ermon, “Generative adversarial imitation learning,” *Advances in Neural Information Processing Systems*, vol. 29, 2016.
- [19] J. Tian, B. Wang, R. Guo, Z. Wang, K. Cao, and X. Wang, “Adversarial attacks and defenses for deep-learning-based unmanned aerial vehicles,” *IEEE Internet of Things Journal*, vol. 9, no. 22, pp. 22 399–22 409, 2021.
- [20] X. Wei, J. Ma, and C. Sun, “A survey on security of unmanned aerial vehicle systems: Attacks and countermeasures,” *IEEE Internet of Things Journal*, 2024.
- [21] Y. Liang, Y. Sun, R. Zheng, and F. Huang, “Efficient adversarial training without attacking: Worst-case-aware robust reinforcement learning,” *Advances in Neural Information Processing Systems*, vol. 35, pp. 22 547–22 561, 2022.
- [22] H. Zhang *et al.*, “Robust deep reinforcement learning against adversarial perturbations on state observations,” *Advances in Neural Information Processing Systems*, vol. 33, pp. 21 024–21 037, 2020.
- [23] C. Tessler, Y. Efroni, and S. Mannor, “Action robust reinforcement learning and applications in continuous control,” in *International Conference on Machine Learning*, PMLR, 2019, pp. 6215–6224.
- [24] C. Axenie and M. Saveriano, “Antifragile control systems: The case of mobile robot trajectory tracking under uncertainty and volatility,” *IEEE Access*, 2023.
- [25] L. Sun, M. A. Makridis, A. Genser, C. Axenie, M. Grossi, and A. Kouvelas, “Antifragile perimeter control: Anticipating and gaining from disruptions with reinforcement learning,” *arXiv preprint arXiv:2402.12665*, 2024.
- [26] C. Pravin, I. Martino, G. Nicosia, and V. Ojha, “Fragility, robustness and antifragility in deep learning,” *Artificial Intelligence*, vol. 327, p. 104 060, 2024.
- [27] M. Jin, “Preparing for black swans: The antifragility imperative for machine learning,” *arXiv preprint arXiv:2405.11397*, 2024.
- [28] Y. Ganin and V. Lempitsky, “Unsupervised domain adaptation by backpropagation,” in *International conference on machine learning*, PMLR, 2015, pp. 1180–1189.
- [29] M. Rostami, “Lifelong domain adaptation via consolidated internal distribution,” *Advances in Neural Information Processing Systems*, vol. 34, pp. 11 172–11 183, 2021.
- [30] S. Sankaranarayanan, Y. Balaji, C. D. Castillo, and R. Chelappa, “Generate to adapt: Aligning domains using generative adversarial networks,” in *Proceedings of the IEEE Conference on Computer Vision and Pattern Recognition*, 2018, pp. 8503–8512.
- [31] M. Long, Z. Cao, J. Wang, and M. I. Jordan, “Conditional adversarial domain adaptation,” *Advances in neural information processing systems*, vol. 31, 2018.
- [32] M. Long, H. Zhu, J. Wang, and M. I. Jordan, “Deep transfer learning with joint adaptation networks,” in *International conference on machine learning*, PMLR, 2017, pp. 2208–2217.
- [33] P. Huang, M. Xu, J. Zhu, L. Shi, F. Fang, and D. Zhao, “Curriculum reinforcement learning using optimal transport via gradual domain adaptation,” *Advances in Neural Information Processing Systems*, vol. 35, pp. 10 656–10 670, 2022.

- [34] J. Xing, T. Nagata, K. Chen, X. Zou, E. Neftci, and J. L. Krichmar, "Domain adaptation in reinforcement learning via latent unified state representation," in *Proceedings of the AAAI Conference on Artificial Intelligence*, vol. 35, 2021, pp. 10452–10459.
- [35] J. Liu, H. Shen, D. Wang, Y. Kang, and Q. Tian, "Unsupervised domain adaptation with dynamics-aware rewards in reinforcement learning," *Advances in Neural Information Processing Systems*, vol. 34, pp. 28784–28797, 2021.
- [36] K. Arndt, M. Hazara, A. Ghadirzadeh, and V. Kyriki, "Meta reinforcement learning for sim-to-real domain adaptation," in *2020 IEEE International Conference on Robotics and Automation (ICRA)*, IEEE, 2020, pp. 2725–2731.
- [37] T. Carr, M. Chli, and G. Vogiatzis, "Domain adaptation for reinforcement learning on the atari," in *Proceedings of the 18th International Conference on Autonomous Agents and MultiAgent Systems*, 2019, pp. 1859–1861.
- [38] Y. Xu, X. Zhong, A. J. J. Yepes, and J. H. Lau, "Forget me not: Reducing catastrophic forgetting for domain adaptation in reading comprehension," in *2020 International joint conference on neural networks (IJCNN)*, IEEE, 2020, pp. 1–8.
- [39] Q. Wang, O. Fink, L. Van Gool, and D. Dai, "Continual test-time domain adaptation," in *Proceedings of the IEEE/CVF Conference on Computer Vision and Pattern Recognition*, 2022, pp. 7201–7211.
- [40] M. Schutera, F. M. Hafner, J. Abhau, V. Hagenmeyer, R. Mikut, and M. Reischl, "Cuepervision: Self-supervised learning for continuous domain adaptation without catastrophic forgetting," *Image and Vision Computing*, vol. 106, p. 104079, 2021.
- [41] M. Rostami, *Transfer learning through embedding spaces*. CRC Press, 2021.
- [42] E. Lecarpentier, D. Abel, K. Asadi, Y. Jinnai, E. Rachelson, and M. L. Littman, "Lipschitz lifelong reinforcement learning," in *Proceedings of the AAAI Conference on Artificial Intelligence*, vol. 35, 2021, pp. 8270–8278.
- [43] A. Perrusquía, "A complementary learning approach for expertise transference of human-optimized controllers," *Neural Networks*, vol. 145, pp. 33–41, 2022.
- [44] A. Perrusquía and W. Guo, "Drone's objective inference using policy error inverse reinforcement learning," *IEEE Transactions on Neural Networks and Learning Systems*, 2023.
- [45] H. Yang, C. Yu, S. Chen, et al., "Hybrid policy optimization from imperfect demonstrations," *Advances in Neural Information Processing Systems*, vol. 36, 2024.
- [46] J. Ramírez, W. Yu, and A. Perrusquía, "Model-free reinforcement learning from expert demonstrations: A survey," *Artificial Intelligence Review*, vol. 55, no. 4, pp. 3213–3241, 2022.
- [47] S. Melacci et al., "Domain knowledge alleviates adversarial attacks in multi-label classifiers," *IEEE Transactions on Pattern Analysis and Machine Intelligence*, vol. 44, no. 12, pp. 9944–9959, 2021.
- [48] Y. Zhang and H. Wang, "Adaptive interfered fluid dynamic system algorithm based on deep reinforcement learning framework," in *International Conference on Autonomous Unmanned Systems*, Springer, 2021, pp. 1388–1397.
- [49] B. Ince, V. C. Martinez, P. K. Selvam, I. Petrunin, M. Seo, and A. Tsourdos, "Sense and avoid considerations for safe suas operations in urban environments," *IEEE Aerospace and Electronic Systems Magazine*, 2024.
- [50] K. Liu and B. M. Chen, "Industrial uav-based unsupervised domain adaptive crack recognitions: From database towards real-site infrastructural inspections," *IEEE Transactions on Industrial Electronics*, vol. 70, no. 9, pp. 9410–9420, 2022.
- [51] H. Huang, A. V. Savkin, and C. Huang, "Decentralized autonomous navigation of a uav network for road traffic monitoring," *IEEE Transactions on Aerospace and Electronic Systems*, vol. 57, no. 4, pp. 2558–2564, 2021.
- [52] J. Perolat, B. Scherrer, B. Piot, and O. Pietquin, "Approximate dynamic programming for two-player zero-sum markov games," in *International Conference on Machine Learning*, PMLR, 2015, pp. 1321–1329.
- [53] P. Kamalaruban, Y.-T. Huang, Y.-P. Hsieh, P. Rolland, C. Shi, and V. Cevher, "Robust reinforcement learning via adversarial training with langevin dynamics," *Advances in Neural Information Processing Systems*, vol. 33, pp. 8127–8138, 2020.
- [54] Y.-P. Hsieh, C. Liu, and V. Cevher, "Finding mixed nash equilibria of generative adversarial networks," in *International Conference on Machine Learning*, PMLR, 2019, pp. 2810–2819.
- [55] N. Carlini and D. Wagner, "Towards evaluating the robustness of neural networks," in *2017 IEEE Symposium on Security and Privacy*, Ieee, 2017, pp. 39–57.
- [56] Y. Dong et al., "Boosting adversarial attacks with momentum," in *Proceedings of the IEEE Conference on Computer Vision and Pattern Recognition*, 2018, pp. 9185–9193.
- [57] H. Kim, W. Lee, and J. Lee, "Understanding catastrophic overfitting in single-step adversarial training," in *Proceedings of the AAAI Conference on Artificial Intelligence*, vol. 35, 2021, pp. 8119–8127.
- [58] M. Andriushchenko and N. Flammarion, "Understanding and improving fast adversarial training," *Advances in Neural Information Processing Systems*, vol. 33, pp. 16048–16059, 2020.
- [59] Z. Golgooni, M. Saberi, M. Eskandar, and M. H. Rohban, "Zerograd: Mitigating and explaining catastrophic overfitting in fgsm adversarial training," *arXiv preprint arXiv:2103.15476*, 2021.
- [60] Z. Wang, C. Chen, and D. Dong, "A dirichlet process mixture of robust task models for scalable lifelong reinforcement learning," *IEEE Transactions on Cybernetics*, vol. 53, no. 12, pp. 7509–7520, 2022.
- [61] N. Ferns, P. Panangaden, and D. Precup, "Bisimulation metrics for continuous markov decision processes," *SIAM Journal on Computing*, vol. 40, no. 6, pp. 1662–1714, 2011.
- [62] P. S. Castro, "Scalable methods for computing state similarity in deterministic markov decision processes," in *Proceedings of the AAAI Conference on Artificial Intelligence*, vol. 34, 2020, pp. 10069–10076.
- [63] Y. Li, X. Zhang, Y. Zhu, and Z. Gao, "A uav path planning method in three-dimensional urban airspace based on safe reinforcement learning," in *2023 IEEE/AIAA 42nd Digital Avionics Systems Conference (DASC)*, IEEE, 2023, pp. 1–7.
- [64] S. Chen, Z. Chen, and D. Wang, "Adaptive adversarial training for meta reinforcement learning," in *2021 International Joint Conference on Neural Networks (IJCNN)*, IEEE, 2021, pp. 1–8.
- [65] C. A. Bhardwaj, "Adaptively preconditioned stochastic gradient langevin dynamics," *arXiv preprint arXiv:1906.04324*, 2019.
- [66] L. Luo, Y. Xiong, Y. Liu, and X. Sun, "Adaptive gradient methods with dynamic bound of learning rate," in *International Conference on Learning Representations*, 2018.
- [67] F. Zou, L. Shen, Z. Jie, W. Zhang, and W. Liu, "A sufficient condition for convergences of adam and rmsprop," in *Proceedings of the IEEE/CVF Conference on computer vision and pattern recognition*, 2019, pp. 11127–11135.
- [68] Y. Duan, X. Chen, R. Houthoofd, J. Schulman, and P. Abbeel, "Benchmarking deep reinforcement learning for continuous control," in *International conference on machine learning*, PMLR, 2016, pp. 1329–1338.

APPENDIX A INTERFERED FLUID DYNAMIC SYSTEM

The interfered flow field causes a change in the initial flow field due to the presence of dynamic obstacles. The 3D obstacle is designed as a standard convex polyhedron, as:

$$\Gamma(\mathbf{P}) = \left(\frac{x-x_0}{\check{a}} \right)^{2\check{p}} + \left(\frac{y-y_0}{\check{b}} \right)^{2\check{q}} + \left(\frac{z-z_0}{\check{c}} \right)^{2\check{r}}. \quad (\text{A.1})$$

In this case, $\check{p}, \check{q}, \check{r}, \check{a}, \check{b}, \check{c}$ determine the shape of the convex polyhedron of the obstacle, and (x_0, y_0, z_0) determine centre of the convex polyhedron. If we consider N obstacles in the space, the interfered flow field is represented by a disturbance matrix as:

$$\bar{M}(\mathbf{P}) = \sum_{n=1}^N \mathfrak{w}_n(\mathbf{P}) M_n(\mathbf{P}), \quad (\text{A.2})$$

where \mathfrak{w} is the disturbance weighting factor for the N obstacles defined as:

$$\mathfrak{w}_n(\mathbf{P}) = \begin{cases} 1 & N=1, \\ \prod_{i=1, i \neq n}^N \frac{\Gamma_i(\mathbf{P})-1}{\Gamma_i(\mathbf{P})-1+\Gamma_n(\mathbf{P})-1}. \end{cases} \quad (\text{A.3})$$

Here we define the radial normal vector along the 3D obstacle \mathbf{t}_n as:

$$\mathbf{t}_n(\mathbf{P}) = \left[\frac{\partial \Gamma_n(\mathbf{P})}{\partial x} \quad \frac{\partial \Gamma_n(\mathbf{P})}{\partial y} \quad \frac{\partial \Gamma_n(\mathbf{P})}{\partial z} \right]. \quad (\text{A.4})$$

We consider two vectors $h_{n,1}(\mathbf{P}), h_{n,2}(\mathbf{P})$ which are orthogonal to the radial vector \mathbf{t}_n and also mutually orthogonal to each other, given as:

$$h_{n,1}(\mathbf{P}) = \begin{bmatrix} \frac{\partial \Gamma_n(\mathbf{P})}{\partial y} \\ -\frac{\partial \Gamma_n(\mathbf{P})}{\partial x} \\ 0 \end{bmatrix}^T, \quad (\text{A.5})$$

$$h_{n,2}(\mathbf{P}) = \begin{bmatrix} \frac{\partial \Gamma_n(\mathbf{P})}{\partial x} \cdot \frac{\partial \Gamma_n(\mathbf{P})}{\partial z} \\ \frac{\partial \Gamma_n(\mathbf{P})}{\partial x} \cdot \frac{\partial \Gamma_n(\mathbf{P})}{\partial y} \\ -\left(\frac{\partial \Gamma_n(\mathbf{P})}{\partial x} \right)^2 - \left(\frac{\partial \Gamma_n(\mathbf{P})}{\partial y} \right)^2 \end{bmatrix}^T.$$

The plane S formed by $h_{n,1}(\mathbf{P}), h_{n,2}(\mathbf{P})$ is perpendicular to \mathbf{t}_n . Hence, we can write any unit vector on the plane S as,

$$[\cos \vartheta_n \quad \sin \vartheta_n \quad 0], \quad (\text{A.6})$$

where ϑ_n is the direction coefficient affecting the tangential disturbance. The disturbance matrix while considering a single obstacle is given as:

$$\mathbf{M}_n(\mathbf{P}) = \mathbf{M}_{n1}(\mathbf{P}) + \mathbf{M}_{n2}(\mathbf{P}),$$

$$\mathbf{M}_n = \mathbf{I} - \frac{\mathbf{t}_n(\mathbf{P}) \mathbf{t}_n(\mathbf{P})^T}{|\Gamma_n(\mathbf{P})|^{\frac{1}{\rho_n}} \mathbf{t}_n(\mathbf{P})^T \mathbf{t}_n(\mathbf{P})} + \frac{h_n(\mathbf{P}) \mathbf{t}_n(\mathbf{P})^T}{|\Gamma_n(\mathbf{P})|^{\frac{1}{\zeta_n}} h_n(\mathbf{P})^T \mathbf{t}_n(\mathbf{P})}. \quad (\text{A.7})$$

Here we can define ρ_n and ζ_n using the given formulas,

$$\begin{cases} \rho_n = \rho_0 \cdot \exp \left(1 - \frac{1}{d(\mathbf{P}, P_d) d(\mathbf{P}, O_n)} \right), \\ \zeta_n = \zeta_0 \cdot \exp \left(1 - \frac{1}{d(\mathbf{P}, P_d) d(\mathbf{P}, O_n)} \right). \end{cases} \quad (\text{A.8})$$

Here, $d(\mathbf{P}, O_n)$ represents the distance between the end of the path and the surface of the N -th obstacle, ρ_0, ζ_0 represents

the response coefficient of the obstacle. The dynamic obstacle speed threat is represented as

$$v_{\text{obs}}(\mathbf{P}) = \sum_{n=1}^N \mathfrak{w}_n(\mathbf{P}) \exp \left[\frac{-\Gamma_n(\mathbf{P})}{\Upsilon} \right] v_{\text{obs}}^n(\mathbf{P}). \quad (\text{A.9})$$

where V_n^{obs} is considered as the moving speed of the N th obstacle, Υ is a constant greater than zero.

APPENDIX B STOCHASTIC GRADIENT LANGEVIN DYNAMICS FOR ACTION ROBUST RL

However, solving the mixed Nash equilibrium objective in (12) can result in the solution becoming trapped at a local saddle point, preventing it from reaching the global optimum. To address this, both the agent and adversarial policies are updated by incorporating isotropic gradient noise into the stochastic gradient descent (SGD) process, to minimize the loss functions during the training of the agent and adversarial networks. By adaptively scaling this noise with higher-order curvature measures, such as Fisher scoring, the noise can be preconditioned to enhance convergence properties [65]. When optimizing the loss function by tuning the parameter Θ using SGD, the update equation at each step is given by

$$\hat{g}_s(\Theta_n) \leftarrow \nabla_{\Theta} \mathcal{L}_s(\Theta_n), \quad (\text{B.1})$$

where, $\mathcal{L}_s(\Theta_n)$ represents the stochastic estimate of the loss function. Hence, the update equation can be represented as

$$\Theta_{n+1} \leftarrow \Theta_n - \eta (\hat{g}_s(\Theta_n)), \quad (\text{B.2})$$

where $\eta > 0$ is the learning rate. Incorporating a zero mean Gaussian noise $\mathcal{N}(0, \epsilon)$ with variance ϵ , we obtain,

$$\zeta_n \sim \mathcal{N}(0, \epsilon),$$

$$\Theta_{n+1} \leftarrow \Theta_n - \eta (\hat{g}_s(\Theta_n) + \zeta_n). \quad (\text{B.3})$$

Uniform noise scaling can result in improper parameter update scaling, potentially slowing the training process and consequently converging to suboptimal minima [66]. To address this issue, adaptive preconditioners such as RMSProp [67] are used, which approximates the inverse of the second-order moments of the gradient update through a diagonal matrix. Bhardwaj et al. Bhardwaj et al. [65] proposed an adaptive preconditioned noise approach that leverages a diagonal approximation of the second-order gradient moments, improving the training efficiency of first-order methods. Consequently, noise scaling is adjusted proportionally to accelerate the training as follows

$$\mathbf{C}_n \leftarrow \rho \mathbf{C}_{n-1} + (1 - \rho) (\hat{g}_s(\Theta_n) - \boldsymbol{\mu}_n) (\hat{g}_s(\Theta_n) - \boldsymbol{\mu}_{n-1}),$$

$$\zeta_n \sim \mathcal{N}(\boldsymbol{\mu}_n, \mathbf{C}_n),$$

$$\Theta_{n+1} \leftarrow \Theta_n - \eta (\hat{g}_s(\Theta_n) + \psi \zeta_n). \quad (\text{B.4})$$

In (16), the noise covariance preconditioner scales the noise in proportion to the dimensions exhibiting larger gradients. This method facilitates escape from saddle points and enhances exploration of the policy space, especially when encountering broader loss minima, thereby accelerating convergence and yielding improved solutions. Consequently, the integration of

adaptive noise within the loss function enables the simultaneous optimization of both the critic loss and the loss functions associated with the agent and adversarial policies. If α_i denotes the adversarial contribution, the general action a_i is expressed as follows

$$a' = \alpha \cdot \pi_{\theta}^{\text{agent}}(\Phi') + (1 - \alpha_i) \cdot \pi_{\omega}^{\text{adv}}(\Phi'). \quad (\text{B.5})$$

If we consider a batch of samples $B = \{(\Phi', a', r', \Phi'^{+1}, \mathfrak{d})\}$ from the replay buffer \mathcal{D} , then we compute the critic target y_{targ} as follows

$$y_{\text{targ}} = r' + \gamma(1 - \mathfrak{d}) Q_{\phi_{\text{targ}}}(\Phi'^{+1}, (1 - \alpha_i) \cdot \pi_{\theta}^{\text{agent}} + \alpha_i \cdot \pi_{\omega}^{\text{adv}}). \quad (\text{B.6})$$

Here, ϕ_{targ} represents the parameters of the target critic network and \mathfrak{d} represents the terminal status of the state transitions. Therefore, the target y_{targ} can be utilized to formulate the expected critic loss function as,

$$L(\phi) = \frac{1}{N} \sum_{B=\{(\Phi', a', r', \Phi'^{+1}, \mathfrak{d})\}} (y(r', \Phi'^{+1}, \mathfrak{d}) - Q_{\phi}(\Phi', a'))^2. \quad (\text{B.7})$$

We can also compute the expectations of the loss functions of the agent and adversary policy networks over the experience samples B as,

$$\begin{aligned} \nabla_{\theta} J(\widehat{\theta}, \widehat{\omega}_t) &= \frac{1 - \alpha_i}{N} \sum_{\Phi, a \in B} \nabla_{\theta} \pi_{\theta}^{\text{agent}}(\Phi) \nabla_a Q_{\phi}(\Phi, a), \\ \nabla_{\omega} J(\widehat{\theta}_t, \widehat{\omega}) &= \frac{\alpha_i}{N} \sum_{\Phi, a \in B} \nabla_{\omega} \pi_{\omega}^{\text{adv}}(\Phi) \nabla_a Q_{\phi}(\Phi, a). \end{aligned} \quad (\text{B.8})$$

To optimize the loss functions of the critic and policy, as specified in equations (B.7) and (B.8) respectively, we incorporate the noise into the update equations as specified in (B.3). This approach is taken to update the parameters of the joint critic network ϕ and the agent and adversary policy network $\{\theta, \omega\}$. Let $\mathbf{g} = \{\nabla_{\theta} J, \nabla_{\omega} J\}$, $\boldsymbol{\mu}_t = \{\mu_{\theta}, \mu_{\omega}\}$, $\mathbf{C}_t = \{C_{\theta}, C_{\omega}\}$ represent the gradient, the joint mean value of the parameters, and the covariance matrices, respectively. According to the dynamics of SGLD given in (B.4), the update equation for the agent and the adversary parameter to obtain the mixed Nash equilibrium for the max-min objective in (12) for the k^{th} sample from the buffer at time t , is given as:

$$\theta_t^{k+1} \leftarrow \theta_t^k + \eta \left(\nabla_{\theta} J(\widehat{\theta}, \widehat{\omega}_t) + \psi \xi_t \right), \quad (\text{B.9})$$

$$\omega_t^{k+1} \leftarrow \omega_t^k - \eta \left(\nabla_{\omega} J(\widehat{\theta}, \widehat{\omega}_t) (\Gamma_t) + \psi \xi_t \right). \quad (\text{B.10})$$

Here, ψ represents the noise parameter. The parameters updated with the time t is given by

$$\bar{\omega}_t = (1 - \beta) \bar{\omega}_t + \beta \omega_t^{(k+1)}; \bar{\theta}_t = (1 - \beta) \bar{\theta}_t + \beta \theta_t^{(k+1)}. \quad (\text{B.11})$$

Obtain the parameters for the next time duration as,

$$\omega_{t+1} = (1 - \beta) \omega_t + \beta \bar{\omega}_t; \theta_{t+1} = (1 - \beta) \theta_t + \beta \bar{\theta}_t. \quad (\text{B.12})$$

APPENDIX C ALGORITHMS

A. Algorithm to Generate Adversarial States

Algorithm 1 Generate adversarial state Φ^{adv} for the adaptation of action robust RL Agent using ZeroGrad

Input Current State Φ , Step size α , number of samples N , maximum perturbation ε , Mean value of state μ_{Φ} , Standard deviation of the state σ_{Φ}

Output Adversarial State Φ^{adv}

```

1: for  $j = 1$  to  $N$  do
2:    $\delta_j \sim \text{Uniform}([- \varepsilon, \varepsilon]^d)$ 
3:    $\nabla_{\delta_j} \leftarrow \nabla_{\Phi} J_{\pi}(\Phi_i + \delta_j)$ 
4: end for
5:  $\omega \leftarrow \frac{1}{N} \sum_{j=1}^N \text{sgn}(\nabla \delta_j)$ 
6:  $\nabla_{\delta} \leftarrow 0$ 
7:  $\nabla_{\delta}[\|\omega\| == 1] \leftarrow \nabla_{\delta_1}$ 
8:  $\delta \leftarrow \alpha \cdot \text{sgn}(\nabla \delta)$ 
9:  $\delta \leftarrow \max(\min(\delta, \varepsilon), -\varepsilon)$ 
10:  $\Phi^{\text{adv}} = \Phi + \delta$ 

```

B. Algorithm to Compute TD Error

Algorithm 2 Temporal difference (TD) error of action robust RL Policy

Input Adversarial state $\Phi_{\varepsilon}^{\text{adv}}$ with strength ε , Sampled Batch $B = \{(\Phi_{\text{adv}}^{\varepsilon}, a_{\text{adv}}^{\varepsilon}, r_{\text{adv}}^{\varepsilon}, \Phi', \mathfrak{d})\}$, Robust agent policy $\pi_{\text{agent}}^{\text{tar}}$, robust adversarial policy $\pi_{\text{adv}}^{\text{tar}}$, Critic for the robust RL Q_{AR} , Critic target for the robust RL $Q_{\text{AR}}^{\text{tar}}$,

Output TD error for the robust policy $\text{TD}_{\Phi_{\text{adv}}^{\text{AR}}}$

Initialize: $\Phi_{\text{norm}} = ()$

```

1:
2: for  $j = 1$  to  $N_{\text{samples}}$  do
3:   Obtain the value with adversarial state as  $V_{\text{adv}} = Q_{\text{AR}}(\Phi_{\text{adv}}^{\varepsilon}, a_{\text{adv}}^{\varepsilon})$ .
4:   Obtain the next action using the target policies  $a^{\text{next}} = (1 - \alpha) \cdot \pi_{\text{agent}}^{\text{tar}}(\Phi'^{+1}) + \alpha \cdot \pi_{\text{adv}}^{\text{tar}}(\Phi'^{+1})$ .
5:   Obtain the value based on next observation and action  $V^{\text{tar}} = Q_{\text{AR}}^{\text{tar}}(\Phi'^{+1}, a^{\text{next}})$ .
6:   Obtain the target value  $V^{\text{targ}} = r_{\text{adv}}^{\varepsilon} + (1 - \mathfrak{d}) \cdot \gamma \cdot V^{\text{next}}$ .
7:   Obtain the TD error  $\text{TD}_{\Phi_{\text{adv}}^{\varepsilon}} = (V^{\text{tar}} - V_{\text{adv}}) \cdot (V^{\text{tar}} - V_{\text{adv}}) / \sigma^2$ .
8: end for

```

C. Algorithm for Domain Adaptation for Antifragility

APPENDIX D

PROOFS FOR ANTIFRAGILE ADAPTATION

A. Proof of Lemma 1

As per Kantorovic-Rubinstein duality, for two different transition probability distributions P_k and P_{k+1} , we define the Wasserstein distance while considering the adversarial state $\Phi'_{\varepsilon_{k+1}} \sim P_{k+1}$ and $\Phi'_{\varepsilon_k} \sim P_k$ between them as,

$$\mathcal{W}_1(P_{k+1}, P_k) = \sup_{\text{Lip}(f) \leq 1} \left| \mathbb{E} \left[f(\Phi'_{\varepsilon_{k+1}}) \right] - \mathbb{E} \left[f(\Phi'_{\varepsilon_k}) \right] \right|. \quad (\text{D.1})$$

Algorithm 3 Domain Adaptation for Action Robust RL**Input** TD error from the expert critic \mathbf{TD}_{exp} .**Output** Antifragile Policies

Initialize: Replay Buffer for Adversarial Samples \mathcal{D}_{adv} , Adaptive Critic $Q_{\text{ad}} = Q_{\text{AR}}$, $\pi_{\text{ad}}^{\text{adv}} = \pi_{\text{AR}}^{\text{adv}}$, $\pi_{\text{ad}}^{\text{agent}} = \pi_{\text{rob}}^{\text{agent}}$, $\varepsilon, \Delta\varepsilon$, exploration episodes $N_{\text{exploration}}$.

```

1: while  $\varepsilon < \varepsilon_{\text{max}}$  do
2:   Repeat
3:     Observe adversarial state  $\Phi_{\varepsilon}^{\text{adv}}$  as per Algorithm 1 with
       adversarial strength  $\varepsilon$ .
4:     if  $N_{\text{episodes}} < N_{\text{exploration}}$  then
5:       Select random actions  $a^t = \mathcal{U}(-1, 1)$ .
6:     else
7:       Select the actions according to  $a_{\text{agent}}^{\varepsilon} =$ 
        $\pi_{\theta}^{\text{agent}}(\Phi_{\text{adv}}^{\varepsilon}) + \zeta$ ,  $a_{\text{adv}}^{\varepsilon} = \pi_{\omega}^{\text{adv}}(\Phi_{\text{adv}}^{\varepsilon}) + \zeta'$  where
        $\zeta, \zeta' \sim \mathcal{N}(0, \sigma I)$ .
8:     end if
9:     Execute the action  $a_{\text{adv}}^{\varepsilon} = \alpha \cdot a_{\text{adv}}^{\varepsilon} + (1 - \alpha) \cdot a_{\text{agent}}^{\varepsilon}$  for
       the UAV to navigate the environment.
10:    Observe the reward  $r_{\text{adv}}^{\varepsilon}$ , obtain the next state  $\Phi^{t+1}$ 
       after applying the action  $a_t$  (1), and check whether the
       UAV has arrived its destination using the done signal  $\mathfrak{d}$ .
11:    Store  $(\Phi_{\text{adv}}^{\varepsilon}, a_{\text{adv}}^{\varepsilon}, r_{\text{adv}}^{\varepsilon}, \Phi^{t+1}, \mathfrak{d})$  in the buffer  $\mathcal{D}_{\text{adv}}$ .
12:    Reset the environment if the state  $\Phi^{t+1}$  is terminal.
13:    if its time to update agent and adversary model then
14:       $\omega_t, \omega_t^{(1)} \leftarrow \omega_t, \theta_t^{(1)} \leftarrow \theta_t$ 
15:      for  $k = 1, 2, \dots, K_t$  do
16:        Sample a random minibatch of  $N$  transitions
         $B = \{(\Phi_{\text{adv}}^{\varepsilon}, a_{\text{adv}}^{\varepsilon}, r_{\text{adv}}^{\varepsilon}, \Phi^{t+1}, \mathfrak{d})\}$  from  $\mathcal{D}$ .
17:        Sample the TD error from the expert  $\mathbf{TD}_{\text{exp}}$ .
18:        Obtain the critic value from the sampled ad-
        versarial states  $V_{\text{ad}} = Q(\Phi_{\text{adv}}^{\varepsilon}, a_{\text{adv}}^{\varepsilon})$ .
19:        Obtain the TD error  $\mathbf{TD}_{\text{AR}}$  from the sampled
        adversarial transition experience for the given robust RL
        critic from Algorithm 2.
20:        Update the critic by computing the following
        distributional loss  $\mathcal{L}_{\text{crit}} = \frac{1}{N} \cdot \mathcal{H}_1(\mathbf{TD}_{\text{exp}}, \mathbf{TD}_{\text{AR}})$ .
21:        Update the adversarial policy  $\pi_{\omega}^{\text{adv}}$  and agent
        policy  $\pi_{\theta}^{\text{agent}}$  using the adversarial loss and agent loss
        given in (B.10).
22:        Update the target networks as follows:
            $\phi_{\text{targ}} \leftarrow \tau \phi_{\text{targ}} + (1 - \tau) \phi$ ,
            $\theta_{\text{targ}} \leftarrow \tau \theta_{\text{targ}} + (1 - \tau) \theta$ ,
            $\omega_{\text{targ}} \leftarrow \tau \omega_{\text{targ}} + (1 - \tau) \omega$ ,
           (C.1)
23:      end for
24:      Update  $\{\omega_{t+1}, \theta_{t+1}\}$  as per (B.12).
25:       $t \leftarrow t + 1$ 
26:    end if
27:    until Maximum Episodes Reached.
28:    Obtain the TD error  $\mathbf{TD}_{\text{AR}}$  for the trained critic  $Q_{\text{AR}}$ 
    as per Algorithm 2 for adversarial strength  $\varepsilon = 1.0$ .
29:     $\varepsilon \leftarrow \varepsilon + \Delta\varepsilon$ 
30:     $\mathbf{TD}_{\text{exp}} \leftarrow \mathbf{TD}_{\text{AR}}$ .
31: end while

```

As per Assumption 2, the value function Q is Lipschitz. Thus, if we consider $f(s) = \frac{1}{L_Q} Q(\cdot)$, then we can write the following relation,

$$\begin{aligned} & \left| \mathbb{E}_{\Phi'_{\varepsilon_{k+1}} \sim P_{k+1}} \left[Q_{k+1}^* \left(\Phi'_{\varepsilon_{k+1}} \right) \right] - \mathbb{E}_{\Phi'_{\varepsilon_k} \sim P_k} \left[Q_k^* \left(\Phi'_{\varepsilon_k} \right) \right] \right| \leq \\ & \sup \left| \mathbb{E}_{\Phi'_{\varepsilon_{k+1}} \sim P_{k+1}} \left[Q_{k+1}^* \left(\Phi'_{\varepsilon_{k+1}} \right) \right] - \mathbb{E}_{\Phi'_{\varepsilon_k} \sim P_k} \left[Q_k^* \left(\Phi'_{\varepsilon_k} \right) \right] \right|, \\ & \left| \mathbb{E}_{\Phi'_{\varepsilon_{k+1}} \sim P_{k+1}} \left[Q_{k+1}^* \left(\Phi'_{\varepsilon_{k+1}} \right) \right] - \mathbb{E}_{\Phi'_{\varepsilon_k} \sim P_k} \left[Q_k^* \left(\Phi'_{\varepsilon_k} \right) \right] \right| \\ & \leq L_Q \mathcal{H}_1(P_{k+1}, P_k) \end{aligned} \quad (\text{D.2})$$

B. Proof of Lemma 2

Using the Bellman optimality equation,

$$Q^*(\Phi) = \max_a \left(r + \gamma \mathbb{E}_{\Phi'} \left[Q^*(\Phi') \right] \right) \quad (\text{D.3})$$

Let us consider the following inequality for two real vectors a and b , which can be written as,

$$\begin{aligned} |a| - |b| & \leq |a - b| \\ \max a - \max b & \leq \max(a - b) \end{aligned} \quad (\text{D.4})$$

Hence, using the above inequalities, let us consider two adversarially perturbed states, Φ_{ε_k} and $\Phi_{\varepsilon_{k+1}}$, taking the difference between the value functions,

$$\begin{aligned} & \left| Q^*(\Phi_{\varepsilon_k}) - Q^*(\Phi_{\varepsilon_{k+1}}) \right| \leq \\ & \max |r_{\varepsilon_k} - r_{\varepsilon_{k+1}}| + \\ & \gamma \max \left(\mathbb{E} \left[Q^*(\Phi'_{\varepsilon_k}) \right] - \mathbb{E} \left[Q^*(\Phi'_{\varepsilon_{k+1}}) \right] \right) \end{aligned} \quad (\text{D.5})$$

Considering the Lipschitz property of the reward and the critic function for incremental adversarial state, we can write,

$$\left| Q_{k+1}^*(\Phi_{\varepsilon_{k+1}}) - Q_k^*(\Phi_{\varepsilon_k}) \right| \leq L'_Q d(\Phi_{\varepsilon_{k+1}}, \Phi_{\varepsilon_k}). \quad (\text{D.6})$$

where, $L'_Q = L_r + \gamma L_Q$.

C. Proof of Lemma 3

As per the definition of the TD error it is a functional transformation of the transition distribution. Hence if we define the functional as $T(\cdot)$, then we can write,

$$\mathbf{TD}_k^* = T(P_k), \mathbf{TD}_{k+1}^* = T(P_{k+1}). \quad (\text{D.7})$$

If we consider a general property of the optimal transport theory, then we can write if T is a Lipschitz function from a metric space $\mathcal{X} \rightarrow \mathbb{R}$, and $\mu, \nu \in \mathcal{P}(\mathcal{X})$ are probability measures on that space, then,

$$\mathcal{H}_1(\mu, \nu) \leq L_T \mathcal{H}_1(T_{\#}\mu, T_{\#}\nu), \quad (\text{D.8})$$

where, $T_{\#}\mu$ is the pushforward of μ under T and L_T is the Lipschitz constant of T . Hence, if T is 1-Lipschitz the above relation becomes,

$$\mathcal{H}_1(\mu, \nu) \leq L_T \mathcal{H}_1(T_{\#}P_{k+1}, T_{\#}P_k) \quad (\text{D.9})$$

As we know, $T(P) = \mathbf{TD}^*(P)$, hence we write,

$$\mathcal{H}_1(P_{k+1}, P_k) \leq \mathcal{H}_1(\mathbf{TD}_{k+1}^*(\varepsilon_{k+1}), \mathbf{TD}_k^*(\varepsilon_k)). \quad (\text{D.10})$$

D. Proof of Lemma 4

Considering the dual form of Wasserstein-1 distance with $\Phi'_{\varepsilon_k} \sim P_k$ and $\Phi'_{\varepsilon_{k+1}} \sim P_{k+1}$,

$$\mathcal{W}_1(P_k, P_{k+1}) = \sup_{f \in \text{Lip}_1} \left| \mathbb{E}[f(\Phi'_{\varepsilon_k})] - \mathbb{E}[f(\Phi'_{\varepsilon_{k+1}})] \right|. \quad (\text{D.11})$$

If we define $f(\cdot)$ be the distance between the perturbed state and the transition state as $f(\Phi') = d(\Phi', \Phi_{\varepsilon_k})$. The function is 1-Lipschitz, hence for any state $\Phi'_1, \Phi'_2 \in \mathcal{S}$, we can write,

$$\begin{aligned} & |f(\Phi'_1) - f(\Phi'_2)| \\ & |d(\Phi'_1, \Phi_{\varepsilon_k}) - d(\Phi'_2, \Phi_{\varepsilon_k})| \leq d(\Phi'_1, \Phi'_2). \end{aligned} \quad (\text{D.12})$$

Now if we plug the above relation in the dual form, we can write,

$$|\mathbb{E}[f(\Phi'_{k+1})] - \mathbb{E}[f(\Phi'_k)]| \leq \mathcal{W}_1(P_k, P_{k+1}). \quad (\text{D.13})$$

We can the above terms, $\mathbb{E}[f(\Phi'_k)] \approx 0$ as we are considering a smooth dynamics for the UAV, as it does not allow a drastic change in the state. And $\mathbb{E}[f(\Phi'_{k+1})] \approx d(\Phi_{\varepsilon_{k+1}}, \Phi_{\varepsilon_k})$, as the distribution is centered around $\Phi_{\varepsilon_{k+1}}$. Hence, using these approximations we can write,

$$d(\Phi_{\varepsilon_k}, \Phi_{\varepsilon_{k+1}}) \leq \mathcal{W}_1(P_k, P_{k+1}). \quad (\text{D.14})$$

APPENDIX E BENCHMARKING ALGORITHMS

Benchmarking is performed by evaluating the standard policy gradient algorithm, such as the DDPG, along with its robust variants. An approach involves an agent who intends to execute an action \mathbf{a} , but an alternative adversarial action $\bar{\mathbf{a}}$ is implemented with probability α . Another variant, conceptually similar to the approach described in Section E.II, employs soft probabilistic robust policy iteration (PR-PI) as proposed in [23], rather than solving the mixed Nash equilibrium objective in (19). The final benchmarking strategy involves training the agent to optimize the rewards without directly modifying the policy during training. Instead, an adversarial buffer is utilized, allowing the agent to learn the optimal value function in the presence of adversarial states. A brief explanation of these algorithms is provided in the subsequent subsections.

A. Deep Deterministic Policy Gradient (DDPG)

The action robust RL is replaced by DDPG considering $\alpha = 0$. Hence, the critic target y_{targ} in (B.6) is modified as follows,

$$y_{\text{targ}} = r_t + \gamma(1-d)Q_{\phi_{\text{targ}}}(\Phi', \mu_{\theta}). \quad (\text{E.1})$$

Similarly the policy loss with $\alpha = 0$ shown in (??) to compute the policy parameter θ , will be as,

$$\nabla_{\theta} \widehat{J(\theta)} = \frac{1}{N} \sum_{\Phi \in \mathcal{S}} \nabla_{\theta} \mu_{\theta}(\Phi) \nabla_a Q_{\phi}(\Phi, a). \quad (\text{E.2})$$

Hence, the min-max objective in (19) is replaced with a pure max objective which can be solved using traditional policy gradient methods as outlined in [68].

B. Probabilistic Robust Markov Decision Process

According to [23], PR-MDP is framed as a zero-sum game between an agent and an adversary. In this framework, an optimal probabilistic robust policy is defined with a probability α , where the adversary assumes control and executes the most detrimental actions to account for potential system control limitations and undesirable outcomes. PR-MDP addresses stochastic perturbations within the policy space. When we consider $\alpha \in [0, 1]$ and the 5-tuple MDP outlined in Section , the probabilistic joint policy $\pi_{P,\alpha}^{\text{mix}}$ is considered as

$$\pi_{P,\alpha}^{\text{mix}}(\mathbf{a}|\Phi) \equiv (1-\alpha)\pi(\mathbf{a}|\Phi) + \alpha\bar{\pi}(\mathbf{a}|\Phi). \quad (\text{E.3})$$

The $\pi_{P,\alpha}^{\text{mix}}$ to learn the optimal value function for PR-MDP is obtained using PR-PI as shown in algorithm 1 in [23].

C. Noisy Robust Markov Decision Process

According to [23], NR-MDP also models a zero-sum game between an agent and an adversary, but incorporates perturbations in the action space rather than in the policy space as in PR-MDP. Given π and $\bar{\pi}$ as the policies of the agent and the adversary, respectively, their joint policy $\pi_{P,\alpha}^{\text{mix}}$ as,

$$\pi_{N,\alpha}^{\text{mix}}(\mathbf{a}|\Phi) = \mathbb{E}_{\mathbf{b} \sim \pi(\cdot|\Phi), \bar{\mathbf{b}} \sim \bar{\pi}(\cdot|\Phi)} [\bar{\mathbf{1}}_{\mathbf{a}=(1-\alpha)\mathbf{b}+\alpha\bar{\mathbf{b}}}]. \quad (\text{E.4})$$

The NR-MDP is analogous to the Markov decision process (MDP) used to develop the ensembles, except for the addition of SGLD noise to the loss function, to obtain the mixed Nash equilibrium solution for the objective. The solution to the min-max objective considered here is according to the soft PR-PI method as described in Algorithm 2 in [23].

D. State Adversarial MDP

The SA-MDP formulation benchmarks the antifragile policy against a theoretically grounded robust learning framework that explicitly models adversarial perturbations on the state observations [22]. In this setting, the observed state is no longer the true state s , but a perturbed version $v(s)$ constrained within a bounded perturbation set $B(s)$. The agent's policy operates on the adversarially distorted observation $v(s)$, while the environment transitions according to the unperturbed state dynamics.

SA-MDP defines a modified MDP tuple (S, A, B, R, p, γ) , where $B(s)$ restricts the adversarial perturbations. The core objective is to regularize the policy such that action distributions under perturbed and unperturbed states remain close. The policy regularization term minimizes the total variation or KL divergence between $\pi(a|s)$ and $\pi(a|v(s))$, thus promoting robustness to adversarial state shifts. This regularizer is incorporated into standard actor-critic algorithms like DDPG and PPO, using techniques such as convex relaxation or stochastic Langevin dynamics to solve the inner maximization over perturbation sets.

Unlike methods that directly inject adversarial states into the replay buffer, SA-MDP systematically aligns the policy over the perturbation set, avoiding unstable training and catastrophic forgetting. In our experiments, we implement SA-MDP using convex relaxation as in [22], and benchmark it against

antifragile RL to evaluate its capacity for generalization under severe adversarial conditions, including high-step PGD and spoofing attacks.

E. Meta-Adversarial Reinforcement Learning

We benchmark our antifragile policy against a meta-learning based approach that incorporates adaptive adversarial perturbations during policy training, as proposed in [22]. This method extends the model-agnostic meta-learning (MAML) framework by explicitly integrating adversarial task variations into the inner-loop adaptation. Each task corresponds to a distinct adversarial perturbation level ε , forming a curriculum of adversarial environments.

In this framework, the agent is trained over a distribution of tasks $\mathcal{T} = \{\varepsilon_1, \varepsilon_2, \dots, \varepsilon_K\}$, where each task applies a bounded observation-space perturbation sampled via a generative adversarial network (GAN) conditioned on the current state. For a given task ε_k , the inner loop optimizes the policy parameters θ on a perturbed environment using policy gradient updates. The updated policy θ'_k is then evaluated on the same task, and the meta-objective is constructed by aggregating performance across all tasks:

$$\min_{\theta} \sum_{\varepsilon_k \in \mathcal{T}} \mathbb{E}_{\Phi \sim \mathcal{D}_{\varepsilon_k}} \left[\mathcal{L}(\pi_{\theta'_k}) \right], \quad \theta'_k = \theta - \beta \nabla_{\theta} \mathcal{L}(\pi_{\theta}, \mathcal{D}_{\varepsilon_k}), \quad (\text{E.5})$$

where β is the inner-loop learning rate, and $\mathcal{D}_{\varepsilon_k}$ denotes the adversarially perturbed data distribution for task ε_k .

The adversarial perturbations are generated by a task-conditioned GAN, trained to minimize the expected Q-value of the perturbed state, thereby producing strong but feasible adversarial samples. Unlike static adversarial training methods, this approach dynamically adapts both the agent and the adversary, encouraging robustness through meta-level generalization. The final meta-update aggregates gradients across tasks to optimize the initial parameters θ , enabling fast adaptation to unseen perturbations at test time.

In our implementation, we adopt a first-order approximation of MAML for computational efficiency and train the adversarial generator alongside the agent in alternating steps. This meta-adversarial RL framework is evaluated under both PGD and spoofing attacks to assess its generalization capability under severe and structured perturbations.